THE IONIZATION OF LITHIUM IONS BY ELECTRON IMPACT

A THESIS

Presented to

The Faculty of the Graduate Division

by

William Carl Lineberger

In Partial Fulfillment

of the Requirements for the Degree

Doctor of Philosophy

in the School of Electrical Engineering

Georgia Institute of Technology

April, 1965

In presenting the dissertation as a partial fulfillment of the requirements for an advanced degree from the Georgia Institute of Technology, I agree that the Library of the Institute shall make it available for inspection and circulation in accordance with its regulations governing materials of this type. I agree that permission to copy from, or to publish from, this dissertation may be granted by the professor under whose direction it was written, or, in his absence, by the Dean of the Graduate Division when such copying or publication is solely for scholarly purposes and does not involve potential financial gain. It is understood that any copying from, or publication of, this dissertation which involves potential financial gain will not be allowed without written permission.

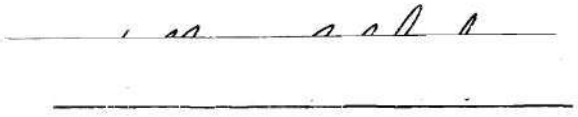

3/17/65
b

THE IONIZATION OF LITHIUM IONS BY ELECTRON IMPACT

Approved:

Dr. J. W. Hooper, Chairman

Dr. E. W. McDaniel

Dr. D. W. Martin

Date approved by Chairman: 4/27/65

ACKNOWLEDGMENTS

It is a great pleasure to express my sincere appreciation to my thesis advisor, Dr. J. W. Hooper, for his continued guidance, assistance and encouragement throughout the performance of this research. The interest and efforts of Dr. Hooper extended far beyond "the call of duty," something for which I am very grateful. I would also like to express my gratitude to Dr. E. W. McDaniel, who was a great aid during the prosecution of the research, and who provided many valuable suggestions during the preparation of this manuscript. This manuscript also benefited greatly from the careful reading and invaluable comments of Dr. D. W. Martin.

It is a pleasure to acknowledge the assistance of Mr. F. M. Bacon during the later developmental phases of the research and during the extensive data collection process. Dr. R. A. Strehlow of the Oak Ridge National Laboratory prepared the synthetic, isotopically purified β-eucryptite ion emitting material; for this service I am very grateful.

I would like to express my appreciation to the Controlled Thermonuclear Research Program, Division of Research, U. S. Atomic Energy Commission for the generous support of this research. Finally, I wish to express my gratitude to the National Aeronautics and Space Administration for their fellowship support during the prosecution of this research.

TABLE OF CONTENTS

TABLE OF CONTENTS (Continued)

LIST OF ILLUSTRATIONS

LIST OF TABLES

ABSTRACT

The absolute cross sections for the single ionization of Li^+ ions by electron impact have been measured as a function of electron energy over the electron energy range from near threshold (75.6 eV) to 800 eV. The measurements were performed with an ultrahigh vacuum, crossed beam facility operating under continuous beam conditions. Numerous checks were performed to evaluate the possible effects of such parameters as the continuous beam measurement technique, beam intensities, beam profiles, space charge, signal-to-noise ratio and ion beam composition. The maximum error in the measurements is estimated to be $\pm$ 12 per cent above 150 eV electron energy, while increasing to $\pm$ 21 per cent at 90 eV. Of this total possible error, an amount $\pm$ 6 per cent is considered systematic. The Li^+ data are compared with the existing relevant experimental and theoretical results.

In the present apparatus, approximately monoenergetic beams of Li^+ ions and electrons are caused to intersect in a well defined collision region, and the composition of the emerging lithium beam is determined with an inclined, parallel plate electrostatic analyzer. The Li^{++} beam current is measured by means of a vibrating reed electrometer operating in the rate-of-charge mode. The ion source is of planar construction and incorporates a platinum gauze thermionic filament

coated with isotopically purified β-eucryptite. The source of electrons is a modified 6L6GC beam power tube. The beam current density distributions are determined by means of a movable slit scanner driven by a micrometer. The various particle currents, particle energies and beam current density distributions represent the experimental information from which the desired cross sections are determined.

Several criteria are developed for assessing the validity of crossed beam measurements, and both the present results and the previously published charged particle-charged particle crossed beam measurements are discussed in the light of these criteria. An expression is developed for the ionization cross section in a crossed beam experiment in terms of the experimental parameters. Several beam pulsing schemes are discussed and compared to continuous beam measurements. Operational procedures for oxide cathodes in demountable vacuum systems are presented, and space charge limitations on useable beam intensities are discussed.

CHAPTER I

INTRODUCTION

Elastic and inelastic collisions involving electrons and heavy particles are of great importance in astrophysics, upper atmospheric phenomena, thermonuclear research, plasma physics, and gaseous electronics. Experimental information concerning such collisions may be obtained either indirectly from swarm studies or directly from beam experiments. The vast majority of direct collision studies have involved the passage of a beam of projectiles through a target gas, and either detection of the reaction products formed in the gas or observation of changes in the composition of the emerging beam. However, the single beam approach is not applicable to the study of many of the reactions of greatest interest -- for example, those involving atoms which normally exist only in molecular form, or those between two species of charged particles. In such cases, it is necessary to study collisions occurring in intersecting beams.

This thesis reports a measurement of the cross sections for single ionization of lithium ions by electron impact over an electron energy range from near threshold (75.6 eV) to 800 eV. The measurements are performed using a crossed beam apparatus operating under continuous beam conditions. The experimental method involves intersecting

approximately monoenergetic beams of lithium ions and electrons in a well defined collision volume. The energy of the primary Li^+ ions is set to be large compared with the energy change experienced by any of these ions in elastic scattering, ionization, or charge transfer events, but their velocity will be low enough that the relative velocity of the two beams is essentially equal to the velocity of the electron beam in the laboratory frame of reference. There are no appreciable electric or magnetic fields in the beam intersection region. Therefore all of the projectile ions, including those which undergo reactions either with electrons or with background gas molecules, travel essentially the same trajectory until the ion beam is separated into its various charge states after passage through the intersection region. Measurement of the composition of the final lithium beam will yield the absolute ionization cross section for the Li^+ projectiles, provided the geometry and intensities of the ion and electron beams are known, and provided that the effects of the background gases are properly assessed. The present research represents the first successful absolute measurements using continuous beams of the cross sections for the ionization of ions by electron impact. The utilization of ultrahigh vacuum techniques was the primary factor enabling the use of continuous beams.

Crossed beam experiments date back at least to 1930, when Funk[1] studied the ionization of sodium and potassium

atoms by electrons. Funk's approach was to intersect a dc beam of atoms from an oven with a dc beam of electrons and collect the ions thus formed in a Faraday cup, in which the atomic beam itself was condensed. Since ionization of the background gas by the electrons gave a contribution to the collected ion current which was about as large as that due to the ionization of the target, Funk's results were not at all accurate. Only with the recent improvements in vacuum technology and development of pulsed beam techniques[2,3] has it been possible to obtain reliable results in crossed beam experiments. The lower base pressures now obtainable result in smaller contributions from the background gas, and, in those cases where it is necessary, beam modulation* permits discrimination of the desired signal from that due to background, since the desired signal occurs at the modulation frequency and at a particular phase with respect to the pulsing signal.

Since the publication of the work cited above, a substantial number of modulated, crossed beam experiments have been performed, principally in this country and in England. The work of greatest relevance to that described here is the measurement of the cross sections for ionization of He^+ ions by electrons in the energy range from 54.4 to 1000 eV. This experiment, performed in 1961 by Dolder, Harrison, and Thonemann[4], was the first study made of the ionization of

---

*See Appendix IV for a detailed discussion of beam pulsing schemes.

positive ions by electron impact. The same group has subsequently measured[5,6] the ionization cross sections for electrons on Ne^+ and N^+. A comparison of their He^+ results with relevant theory was made. At the higher electron energies, where agreement is to be expected, the He^+ cross sections are in good agreement with the theoretical cross sections calculated by Burgess[7,8] and with the scaled experimental results for H atom ionization obtained by Fite and Brackmann[3] and by Rothe, et al[9]. In addition to this work, Latypov, Kupriyanov and Tunitskii in the Soviet Union have recently published measurements[10,11] of the ionization cross sections for electrons incident on several species of ions. Unfortunately, the authors do not appear to have made all of the checks necessary to ensure validity of their results, and it is likely that large errors are present in their results. The publications of these two groups, who have produced the only previously reported charged particle-charged particle crossed beam measurements, are considered in detail in Chapter II.

In principle, accurate quantum mechanical calculations could be made for any atomic collision process provided a complete set of wave functions for the collision partners is known. However, wave functions adequate for the description of collision phenomena are not known at the present time except for hydrogenic atoms and ions. As a consequence of this fact and the almost intractable infinite set of equations describing a collison process, recourse must be made in the calculations to approximations whose a priori validity is

very difficult or impossible to assess. In order to evaluate the validity of these approximations, it is imperative to have available a body of reliable experimental cross section data for "simple" systems to compare with these calculations. If some insight into the range of validity of a given approximation can thus be obtained, it becomes possible to make reliable theoretical estimates on collision processes which are not amenable to experimental investigation. The only "simple" ionic specie for which experimental electron impact ionization data have been available previously is the helium ion; the lithium ion data presented here thus represent a significant addition to such data.

The ionization cross sections for lithium atoms and ions are also of astrophysical interest. Appreciable amounts of lithium (produced by nuclear synthesis) are known to be present in the atmospheres of certain types of stars[12,13]. The ratios of the intensities of lines in the lithium spectra depend on the excitation, ionization, and recombination cross sections for lithium atoms and ions as compared to the cross sections for the other species present. Detailed knowledge of the ionization cross sections of Li and Li^+ would be of considerable interest in comparing the LiI and LiII lines in the solar chromosphere and in the corona in order to deduce reliable electron temperatures.

A practical incentive for obtaining information on the ionization of lithium ions by electrons is related to the use of lithium arcs in certain thermonuclear devices. High current

carbon arcs have been used to provide a target for dissociation of injected molecular ion beams, but the large cross sections for charge transfer between deuterium ions and carbon ions make the use of the carbon arc look unpromising. The charge transfer losses are considerably smaller for lithium arcs, particularly if the lithium atoms in the arc are completely stripped of electrons. The ionization of lithium atoms in the arc occurs predominantly by electron impact, and multiple ionization usually involves successive collisions. The electrons in the lithium arc have energies ranging from a few tens of electron volts to over 100 electron volts. Therefore, the determination of the cross sections for ionization of lithium ions, as well as atoms, by low energy electrons may be of value in controlled thermonuclear research.

CHAPTER II

CHARGED PARTICLE-CHARGED PARTICLE CROSSED BEAM EXPERIMENTS

This chapter concerns some general features of charged particle-charged particle ionization experiments. The results will be specialized to the single ionization of lithium ions in a later chapter. An expression for the ionization cross section in terms of the experimental parameters is presented. The advantages and difficulties associated with these experiments are discussed. In this connection several criteria are set forth to evaluate the performance of an experimental apparatus. Published data are briefly reviewed and discussed in the light of these criteria.

Expression for the Cross Section in Terms of Experimental Parameters

In an electron-ion crossed beam ionization experiment, beams of ions and electrons are caused to intersect in a collision region. As a consequence of the much greater mass of the ion, it is possible to ensure that any interaction with the electron beam results in small angle scattering of the ions. Thus those ions which have undergone interactions with the electrons emerge from the collision region with essentially the same velocity as that of the unreacted ions. In the case of electron impact ionization of the ions,

the reacted component can be separated from the primary beam by means of either magnetostatic or electrostatic charge state analyzers. The electron current, the currents of reacted and unreacted ions, and the various projectile energies are experimentally observed quantities from which the desired cross sections might be calculated. We shall find that it is also necessary to know the current density distributions of both beams in order to determine the cross sections absolutely.

Consider a monoenergetic electron beam and a monoenergetic singly ionized ion beam traveling parallel to the X and Y axes, respectively, of a rectangular Cartesian coordinate system. Let V_i and V_e be the ion and electron velocities. If both beams are sufficiently tenuous that multiple collisions can be neglected, then it can be shown* that the cross section for the second ionization of the ions is given by

$$\sigma_{12} = \frac{eV_iV_e}{2(V_i^2 + V_e^2)^{\frac{1}{2}}} \frac{I^{++}}{\int_{-\infty}^{\infty} i^+(z)j(z)dz} \qquad (1)$$

where $i^+(z)dz$ and $j(z)dz$ are the ion and electron currents passing through the region z to z + dz, I^{++} is the total current of doubly-charged ions produced by electron impact, and e is the magnitude of electronic charge. A more convenient form for this expression is

---

*This expression is derived in Appendix I.

$$\sigma_{12} = \frac{I^{++}}{JI^{+}} \frac{eV_i V_e}{2(V_i^2 + V_e^2)^{\frac{1}{2}}} F \qquad (2)$$

where

$$F = \frac{I^{+}J}{\int_{-\infty}^{\infty} i^{+}(z)j(z)dz} = \frac{\int_{-\infty}^{\infty} i^{+}(z)dz \int_{-\infty}^{\infty} j(z)dz}{\int_{-\infty}^{\infty} i^{+}(z)j(z)dz} \qquad (3)$$

and I^{+} and J are the total ion and electron currents. With the exception of the factor F, Eq. (2) involves directly measurable experimental quantities. The factor F is a form factor involving the current density distributions of the ion and electron beams; it may be evaluated approximately* with the use of scanning slits on both beams. The most obvious way of doing this is shown in Figure 1. The movable slit scanner is completely removed from the beams to permit measurement of I^{++}, J, and I^{+}. The scanner is then lowered across the beams, as shown in the figure, thereby allowing measurement of the beam current distributions. It is important to note that the scanner provides beam profile information <u>near</u> but not <u>in</u> the collision region, and that it essentially negates the space charge influence of one beam upon the other. These points are discussed at length in the section on difficulties associated with crossed beam experiments.

---

*See Appendix I.

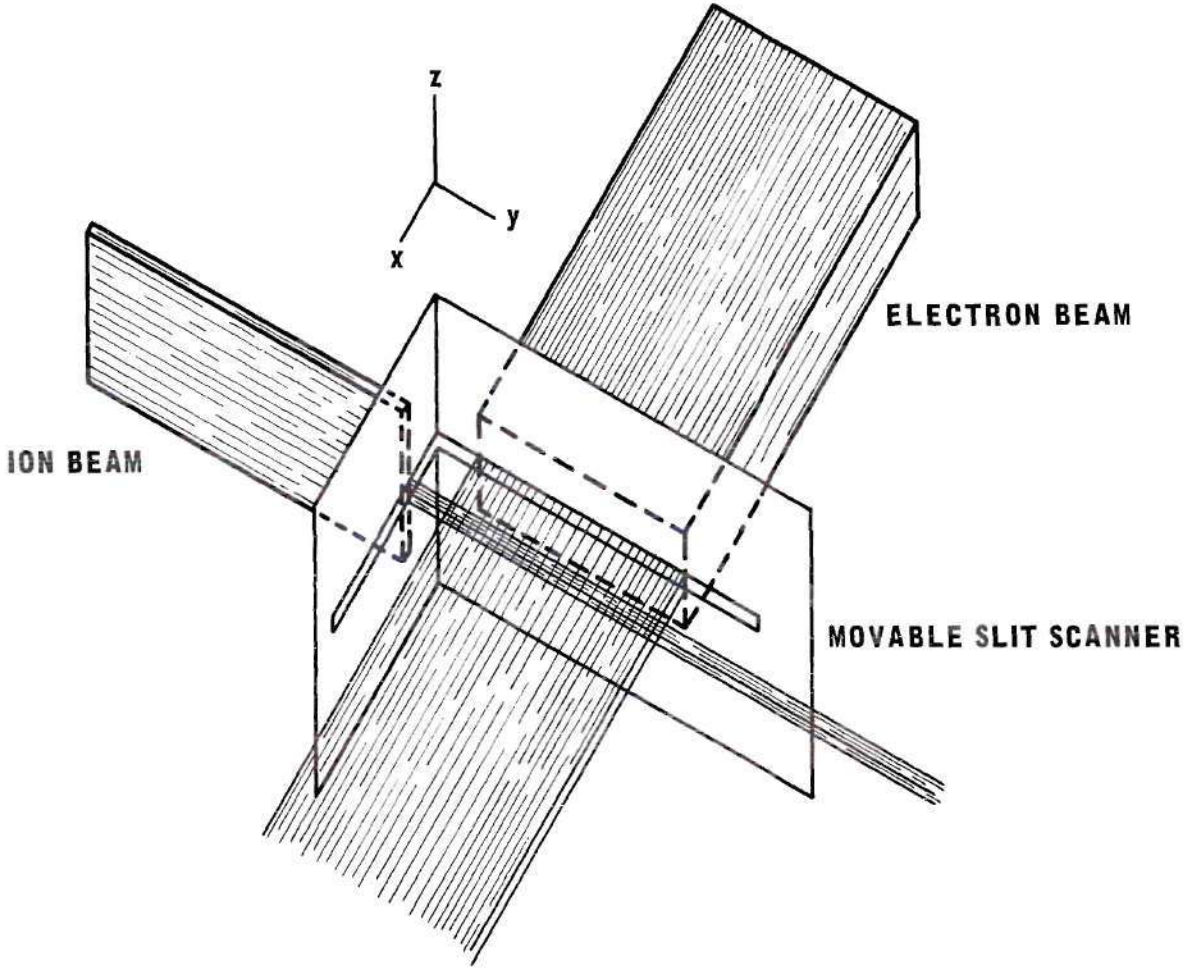

Figure 1. Use of a Movable Slit Scanner to Determine Beam Profiles.

In an ordinary crossed beam experiment, the electron velocity V_e is much greater than the ion velocity V_i. Under this condition the relative velocity of approach of an ion and an electron is essentially the electron velocity; the total energy in the center-of-mass reference frame is very nearly equal to the laboratory energy of the electron. Since the cross sections should be a function only of the total center-of-mass energy, the measured cross sections should remain constant as the ion energy is varied, provided that the electron energy is fixed. For a given electron energy the measured cross sections should also be independent of changes in the electron beam intensity, the ion beam intensity, and the form factor F. As will be seen in a later section, the variation of each of these parameters provides a valuable check on some aspects of the performance of the experimental apparatus.

Advantages of Crossed Beam Techniques

As stated in the introduction, the vast majority of direct collision studies have involved the passage of a beam of projectiles through a target gas, and detection of the reaction products formed in the gas or observation of changes in the composition of the emerging beam. However, the single beam approach is not applicable to the study of many of the reactions of greatest interest — for example, those involving atoms which do not normally exist stably as single atoms, or those between two species of charged particles. In such

cases, it is necessary to study collisions occurring in intersecting beams.

The essential factors in a crossed beam experiment differ in several important respects from those of a single beam experiment. A single beam ionization experiment requires an absolute measurement of the target gas pressure, as well as of the particle currents, in order to determine the absolute ionization cross section. A crossed beam ionization experiment requires no such pressure measurement; the cross section is determined absolutely provided only that all the particle currents be known absolutely, and that the form factor F be determined. The present primary standard for low pressure measurement is the McLeod gauge. This gauge must be carefully used if precise measurements are to be obtained. The inherent accuracy of McLeod gauge measurements is also suspect; recent studies[14,15,16] of the pumping effect[17] of the mercury in the gauge have cast serious doubt on the validity of many experiments which used the McLeod gauge to measure pressure. At least until this matter is resolved, it is a distinct advantage to be able to determine absolute cross sections without the necessity for absolute pressure measurements.

Difficulties Associated with Charged Particle-Charged Particle Crossed Beam Experiments

The following remarks will pertain to experimental difficulties primarily associated with crossed beam experiments. Thus many problems common to all atomic collision experiments will be omitted. Among those to be omitted are such topics

as Faraday cup efficiency, particle loss from beams, beam energy distributions, and accuracy of the measurement instrumentation.

Low Reaction Rates

The fact that both beams are composed of charged particles imposes a space charge restriction on the maximum particle number density attainable in either beam. This restriction results in a severe limitation on the magnitude of the reaction component relative to those of the interacting beams. If one were investigating, for example, charge stripping of He^{+} on H_2, the H_2 pressure in the collision region could be increased to just below the point that multiple collisions of the ion beam with the target gas become appreciable. The He^{++} signal component might be of the order of one per cent of the magnitude of the primary beam. In an electron-ion crossed beam experiment, however, space charge limitations on the electron beam preclude obtaining such high conversion efficiencies. Over the electron energy range from 50 eV to 500 eV, space charge considerations* limit the permissible electron current densities to the order of milliamperes per cm^2. Such a current density represents an electron number density in the collision region which is far below the usual target number densities employed in single beam experiments. This fact is responsible for the low reaction rates typical of charged particle-charged particle crossed beam experiments.

---

*See Appendix V for a discussion of space charge limitations.

The measurements performed in the present research furnish a typical example. At an ion energy of 1 keV and with a 300 eV, 1.0 ma. electron beam (an electron energy near the peak of the cross section), about 4 Li^{+} ions in 10^{9} are converted to Li^{++} ions. Thus the ion beam emerging from the collision region contains two components differing in intensity by about 8 orders of magnitude. This difference in intensity requires that careful attention be paid to the ion beam optics in order to prevent stray particles from the primary beam completely obscuring the smaller beam of the reaction product.

Since typical primary ion beam intensities are on the order of a few tenths of a microampere, the reaction product current will be in the 10^{-15} ampere range. The only current measuring instrument presently capable of measuring such currents accurately is the vibrating capacitor electrometer. Particle multipliers and solid state detectors could be employed as amplifiers for measuring this current, but their gain is generally not sufficiently constant to permit accurate absolute current measurements. A multiplier could also be used in a pulse counting mode, but, again, present multipliers are incapable of counting 1 keV ions with 100 per cent efficiency. The vibrating capacitor electrometer was selected for use in this experiment; details on its use appear in the next chapter.

Interactions with Background Gas

Charged particle-charged particle crossed beam

experiments are further complicated by the fact that the number densities of the particles in the beams are comparable to the number density of the residual gases, even in an ultrahigh vacuum (~10^{-9} Torr) system. In general, the interaction of the primary ion beam with the residual gases cannot be ignored. In an electron ionization crossed beam experiment the most troublesome of these interactions is that of charge stripping:

$$X^+ + R \rightarrow \begin{matrix} X^{++} + R + e \\ X^{++} + R^+ + 2e \end{matrix}$$

where X^+ is one of the primary ions, and R is a residual gas molecule. Such stripping usually results in only a small deflection of the energetic ion, thereby allowing the charge-stripped ion to remain a part of the primary ion beam. If the stripping occurs in a field free region near the region of intersection with the electron beam, then the charge-stripped ion is indistinguishable from doubly-ionized ions produced by electron impact; the charge-stripped ions thus can contribute to the measured current of doubly-ionized particles produced by electron impact.

The intensity of the charge-stripped component is directly proportional to the number density of the residual gases (provided the composition of the gas remains unchanged), and hence to the chamber pressure. Therefore, in order to determine the electron ionization component of the

doubly-ionized beam, it is not necessarily sufficient to take the difference between I^{++} with the electron beam on and I^{++} with the electron beam off. In order for this difference to be a valid measure of the electron ionization component of the beam, assurance must first be made that either

(1) the chamber pressure is unaffected by turning the electron beam "on or "off," or

(2) the charge-stripped component is sufficiently small relative to the electron ionization component that changes in the charge-stripped component attendant with turning the electron beam on and off do not make a significant difference in the computation of the net electron ionization current.

Requirement (1) can be met by pulsing the electron beam at a frequency sufficiently high that the chamber pressure cannot change appreciably between the "on" and "off" times of the pulses. A more useful approach, however, is to pulse both the ion and electron beams. By varying the relative phases of the two beams, they can be made to cross the collision region either in time coincidence or time anti-coincidence. The difference between the I^{++} currents measured in these two modes yields the electron-impact-ionization current. Such a scheme has been employed in the experiments by Dolder, Harrison, and Thonemann.[4,5,6] This beam pulsing scheme and other possible schemes are considered in detail in Appendix IV.

Since the pressure will certainly rise when the electron beam is turned on, the difference between I^{++} with both beams on and I^{++} with only the ion beam on will be greater than the electron-impact-ionization current by an amount equal to the increase in the charge-stripped ion current produced by the pressure increase. It is possible, however, to assess whether a significant error results from assuming that the charge-stripping component of this difference measurement is much less than the electron-impact-ionization component. At electron energies below the threshold for electron impact ionization of the ions, the electron-impact-ionization component of this difference measurement will be zero. The charge-stripping component is not a serious source of error provided that the difference measurement below threshold yields a result which is insignificant compared with that found well above threshold. This statement assumes, of course, that the below threshold measurements are made with ion and electron beam intensities which are typical of measurements above threshold. In order for this charge-stripping component not to be a serious source of error, and thus for cross sections to be able to be measured without the use of pulsing techniques, it will generally be necessary to reduce the operating pressure of the experimental apparatus to 10^{-8} Torr or lower. Provided only that the measured cross section is zero below threshold, this continuous beam measurement scheme is equal or superior to any pulsing scheme. This last statement is

perhaps the most important conclusion reached in Appendix IV, which contains a general discussion of pulsed beam techniques.

Space Charge and Beam Profiles

As indicated previously, the absolute measurement of the cross section requires knowledge of the current density distributions of the intersecting beams. Some form of beam scanner must be employed to obtain this information, from which the form factor F may be calculated. The form factor determination is subject to error from two principal sources, namely

(1) the profile determinations are made a short distance away from the beam intersection region rather than within this region, and

(2) the beam profiles determined with the scanner may not reflect the alterations in the beam profiles at the intersection region which are produced by the macroscopic space charge influence of one beam upon the other.

We shall now consider errors in form factor determinations resulting from each of these sources, and formulate checks for the presence of these possible errors. Criteria will be developed for determining when the beam profiles are satisfactory. Finally a "double" scanner scheme is proposed which can unambiguously determine the presence of form factor errors.

The fact that the scanner is located away from the interaction region permits form factor errors resulting from

space charge expansion of the beams and from tilt of the beams. If, in Figure 1, either beam is not traveling exactly parallel to the X-Y plane, then the relative positions of the current density distributions as determined by the scanner are not the same as their relative locations at the interaction region. It is therefore desirable to be able to show that the form factor remains unchanged upon translating one of the measured profiles a small distance $\pm \Delta z$ with respect to the other. A large tilt in one of the beams can be detected in the following manner: The scanning slit is set to a central position in the beam current distributions, thereby restricting the heights of the ion and electron beams to that of the scanning slit. A check is made to determine whether any electron impact ionization signal is present. Provided that any such signal can be detected, the relative shift in the beam profiles is less than the height of the scanner slit, approximately. In this case, the form factor need be invariant only for a relative profile shift of $\pm$ h, where h is the height of the scanner slit.

Both beams will expand as a result of their space charge. The electron beam expansion will generally be much greater than that of the ion beam, as a consequence of its normally much greater space charge. The electron beam height observed with the scanner will consequently be somewhat less than the actual electron beam height at the interaction region. In order to avoid errors arising from this source, the ion

beam should be taller than the electron beam. If the ion beam is both reasonably uniform and taller than the electron beam, then the measured form factor will be close to the actual form factor, namely that for a somewhat "spread out" electron beam. This point can be checked by simply calculating the form factor for an electron beam profile which has been altered to simulate space charge spread, and verifying that the resulting form factor is the same as the form factor obtained for the unaltered beam. Since the space charge spread of the electron beam is proportional to the electron beam intensity, this point can also be checked by verifying that the measured cross section is independent of the electron beam intensity. When the ion and electron beams are of the same height, significant errors will almost surely arise from this source.

In addition to these self-space-charge effects, the space charge influence of one beam upon the other can create errors in profile determination. The electron beam number density is both large and also much greater than that of the ion beam; consequently the electron beam can significantly influence the ion beam, whereas the effect of the ion beam upon the electron beam is small. For example, if there are losses from the ion beam resulting from divergence in the "z" direction with no electron beam, then the presence of the electron beam can reduce or eliminate these losses. The ion beam tends to move to those regions where the electron beam

is most dense. Since the scanner blocks off most of both beams, this space charge interaction is not reflected in the measured profile. This difficulty is not eliminated by simply having an ion beam whose measured profile is both uniform and taller than that of the electron beam. Such a beam will still develop a more dense region in the vicinity of the electron beam, and the measured profile will be in error. The ion deflection is not serious, however, if it can be shown that the measured cross section is independent of ion energy. Since the ion deflection is reduced as the ion velocity increases, constancy of the measured cross sections as the ion energy is varied implies that deflection of the ion beam by the electron space charge is not significantly affecting the measured beam profiles.

The question naturally arises as to what characterizes a "good" beam profile. Other workers[4] have defined a form factor in the following manner. Let both beams be restricted by apertures to the range $0 \leq z \leq h$. Then, after multiplication and division by h, Equation (2) may be rewritten as

$$\sigma_{12} = \frac{I^{++}}{I^{+}J} \frac{heV_i V_e}{2(V_i^2 + V_e^2)^{\frac{1}{2}}} F' \qquad (4)$$

where

$$F' = \frac{\int_0^h i^+(z)dz \int_0^h j(z)dz}{h \int_0^h i^+(z)j(z)dz} \qquad (5)$$

The form factors F and F' differ only trivially. However, the expression for the cross section which employs the form factor F' appears to depend on the height of the beam defining apertures, "h." Such a dependence, of course, does not exist, but the appearance of h in the cross section expression can be misleading. In order to avoid this possible confusion, the first expression for the cross section will be employed here. We note that if either beam is uniform, the form factor F' is equal to unity. Unfortunately, a form factor of unity does not insure "good" profiles because any of the following problems might still be present.

(1) The ion and electron beams might be of the same height, thus yielding errors as a result of space charge spread of the electron beam.

(2) The convergence of the ion beam by the electron beam is not assessed. It still remains to be shown, as an additional check, that the measured results are independent of ion energy.

(3) The beams may not be uniform. There exist grossly nonuniform beams for which the form factor F' is unity.

The conclusion is, therefore, that a single number cannot be used as a measure of the quality of the beam profiles.

A better scheme is to regard the form factor as a functional defined on the ion and electron beam current density distributions, $i^+(z)$ and $j(z)$, respectively. A "good" profile is then one whose form factor is relatively constant with respect to certain variations in $i^+(z)$ and $j(z)$. These variations are those which arise from or simulate tilt and space charge spreading of the electron beam. In addition, the measured cross sections must be independent of ion energy. If these criteria are met, then the beam profiles can be said to be "good." It is perhaps worth noting that the effects mentioned in this discussion are not necessarily academic exercises, too small ever to be noticed. It has been possible to observe each of the effects discussed above in the experimental apparatus described in this report.

Another type of beam scanning arrangement is possible, however, which permits a direct check on all of the above effects. Referring to Figure 1, a second beam scanner is required which will intercept the beams just <u>after</u> passing through the collision region.

If a scan is made by one scanner, followed subsequently by a scan with the second scanner, and if the two form factors calculated from these scans turn out to be essentially the same, then the profile determination will not be a source of error. This "double" scanner arrangement has not yet been incorporated into any experimental apparatus, but it certainly appears to be a worthwhile feature for a future experiment.

Excitation State of Ion Beam

In order for an experiment to yield unambiguous results it is necessary to know the state of excitation of the ion beam. The only significant contamination will usually arise from metastable states, since the ion source can be sufficiently removed from the interaction region to permit the decay of ordinary excited states before the interaction occurs. Metastable contamination is, however, a serious problem, for in an ionization experiment the cross section for ionization of a metastable ion can be much greater than that of the ground state ion. In addition, the threshold energy for ionization of the metastable ion lies below that of the ground state ion.

The presence of significant metastable ion contamination can be readily determined by measuring the ionization cross section at an electron energy just below the ground state ionization threshold but above the metastable state ionization threshold. If the resultant cross section is zero to within the experimental error, then any metastable component of the primary ion beam does not present a serious problem. In this connection thermionic ion sources are to be preferred over electron impact sources, since the thermionic emission process[18] precludes the emission of appreciable numbers of ions in excited states. Thermionic ion sources are discussed in more detail in the next chapter.

Review of Charged Particle-Charged Particle Crossed Beam Research

In the preceding section, a number of difficulties present in crossed beam experiments have been discussed. From these difficulties emerge several criteria which can be utilized to assess the validity of a crossed beam experiment. These criteria are summarized below.

(1) The measured cross sections should be independent of the electron beam intensity.

(2) The measured cross sections should be independent of the ion beam intensity.

(3) The measured cross sections should be independent of changes in the beam profiles.

(4) The measured cross sections should be independent of changes in the ion beam energy.

(5) The measured cross sections should ideally be zero below the threshold energy for the process being studied. If this is not the case, then a plausible explanation for the nonzero result must be given, together with a means for extracting the desired cross section from the actual measurements.

(6) If beam pulsing techniques are not utilized, then it must be demonstrated that ion beam interactions with the residual gases were properly taken into account.

As of this date two groups have published results of charged particle-charged particle crossed beam experiments. These

groups are Dolder, Harrison and Thonemann[4,5,6] at the Atomic Energy Research Establishment in England, and Latypov, Kupriyanov and Tunitskii[10,11] at the L. Ya Karpov Physico-Chemical Institute in the Soviet Union. The remainder of this section will be devoted to a review of their experimental results in the light of the criteria summarized above.

Dolder, Harrison and Thonemann

The work of Dolder, Harrison and Thonemann (henceforth referred to as DHT) is of great importance. Their study of the ionization of helium ions by electron impact[4] represents the first successful charged particle-charged particle crossed beam experiment. DHT devised a beam pulsing scheme which permitted successful operation of their apparatus at 10^{-6} Torr. This scheme is discussed in detail in Appendix IV. The apparatus was subsequently utilized to study the electron impact ionization of atomic nitrogen ions[6] and neon ions[5].

In all of their experiments, the measured cross sections were shown to be independent of electron and ion beam intensities [criteria (1) and (2)]. It is not possible to determine from their publications whether the criteria relating directly to beam profiles [(3) and (4)] were satisfied. However, their typical beam current density distributions,* together with their ion energy of 5 keV, indicate that these criteria were also satisfied. There remains only the question of the measured cross section below threshold. Since

*Private communication from Dr. M.F.A. Harrison.

each of the three ions studied presented different problems in this respect, they will be considered separately.

e + He^+. The He^{++} ionization signal current was not zero below threshold as a result of the space charge of the electron beam converging some charge-stripped He^{++} ions into the He^{++} detector, these ions being ones which would have missed the He^{++} detector without the converging effect of the electron beam. The result is that a He^{++} current component appears in phase with the pulsed electron beam; this component is not related to electron impact ionization, and hence the measured cross section could be nonzero at an electron energy below the electron impact ionization threshold. DHT assumed that all of the measured He^{++} signal current below threshold was a result of the above process. Simple space charge theory suggests that the size of this component should be proportional to the electron number density, a fact not inconsistent with their results below threshold. On this basis a correction curve was deduced which reduced the measured cross sections to zero below threshold, and, upon extrapolation, provided a correction to the measured results above threshold. The estimated accuracy of determination of the correction term is $\pm$ 30 per cent. The size of this correction varies from -100 per cent at threshold (54.5 eV) to about -3 per cent at 1000 eV. The correction is less than -10 per cent above 100 eV. Thus, while details of the ionization cross section are not clear near threshold, the

uncertainty diminishes rapidly with increasing electron energy. Above 175 eV electron energy, DHT quote a maximum total error of ± 10 per cent in their experimental results.

e + N^+. This measurement yielded a large cross section below threshold, apparently as a result of electron impact dissociation of N_2^{++} into N^{++}, the N_2^{++} being a source produced contaminant in the primary N^+ ion beam. A correction curve for this process is again proposed, but the corrections here are larger and on less certain grounds than the He^+ corrections. The authors do not assign error brackets for this experiment.

e + Ne^+. This experiment turned out to be the least complicated crossed beam ionization experiment carried out by DHT. The measured cross sections were zero below threshold (41 eV), and the ionization signal currents were larger and more easily separated from the background. The authors quote errors of ± 8 per cent above 90 eV.

DHT employed pulsed beam techniques in all of their measurements. Their ionization signal to background current ratio was never greater than unity, as a consequence of the 10^{-6} Torr operating pressure in their vacuum chamber. Their experiments represent a very important and pioneering effort in charged particle-charged particle crossed beam research.

Latypov, Kupriyanov and Tunitskiĭ

In two papers[10,11] Latypov, Kupriyanov and Tunitskiĭ (hereafter referred to as LKT) reported measurements of

electron impact ionization of Hg^+, Xe^+, Kr^+, A^+, Ne^+, Hg^{++}, Xe^{++}, Kr^{++}, and A^{++} ions. Unfortunately, their papers do not present evidence that any of the criteria previously set forth were met. From the LKT publications, however, the following conclusions can be drawn.

LKT did not measure beam current density distributions for any of their ions. This fact, coupled with the fact that the ion and electron beams were defined by apertures to the same height, must result in significant errors in the absolute magnitudes of the cross sections. It is likely that even the shape of their curves is somewhat in error as a result of this omission. LKT did not pulse their beams, and did not utilize ultrahigh vacuum apparatus to reduce the charge-stripped ion currents to a negligible level. Since they present no results below threshold, their use of continuous beams is suspect.

The electron bombardment ion source used by LKT produced many ions in excited states. They present curves showing that the measured cross sections may vary by a factor of three as the electron energy in the ion source is varied. Thus a large contamination of excited ions is often present, making interpretation of their results more difficult.

Very little information was presented for many of the ions that LKT have investigated. For example, the total information presented for electron impact ionization of Ne^+ is that, at an unstated electron energy near the maximum of the

ionization cross section, the ionization cross section is 4×10^{-17} cm^2. Curves are presented only for Hg, Xe, and Kr, each of which contains an unknown contamination of excited ions in the primary beam.

The authors present insufficient experimental data to enable judgement to be passed on any other facets of performance of their apparatus. It is apparent, however, that large errors are present, and that the LKT measurements can at best be called relative.

CHAPTER III

EXPERIMENTAL APPARATUS

The objective of this research was the measurement of the cross sections for single ionization of Li^+ ions by electron impact as a function of electron energy over the electron energy range from near threshold (75.6 eV) to 800 eV. The measurements were made without resorting to pulsed beam techniques. The experimental method involves intersecting a beam of lithium ions with a beam of electrons in a well defined collision region. The lithium ion energy is set sufficiently high to ensure that particles are not scattered out of the ion beam as a result of interaction with the electron beam. Upon exiting from the interaction region, the ion beam is separated into its various charge states by means of an electrostatic deflection system. Knowledge of the various particle energies and currents, together with the current density distributions of the ion and electron beams, enables calculation of the absolute ionization cross section by means of Equation (2). The utilization of continuous rather than pulsed beams requires that the experiment be performed in an ultrahigh vacuum environment.

A schematic diagram of the experimental apparatus is presented in Figure 2. The major components of the apparatus are readily recognized from the preceding description. In

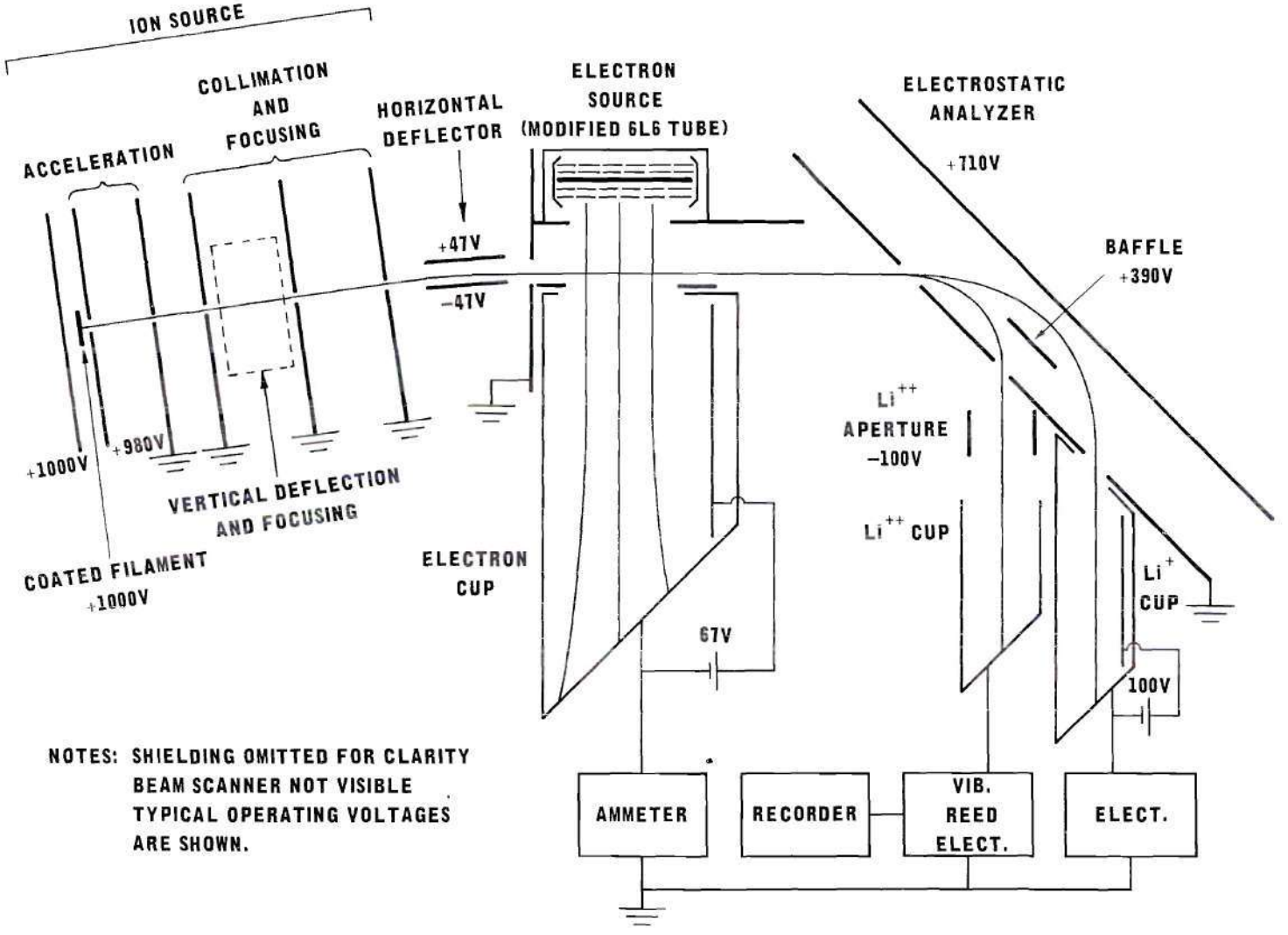

Figure 2. Schematic Diagram of the Experimental Apparatus. The operation of each component is explained in the text.

the diagram the beam scanner, which intercepts the ion and electron beams just prior to their intersection, is not visible. In addition, the ion source details and the extensive shielding of the Li^{++} Faraday cup have been omitted for clarity. An overall view of the experimental apparatus is shown in Figure 3. The vacuum system control instrumentation is on the left of the vacuum chamber, while the instrumentation for the actual experiment is on the right. The remainder of this chapter is concerned with a detailed description of the construction and operation of each of the major components of the experimental apparatus.

Vacuum System

The vacuum enclosure is an all stainless steel bakable chamber 21 inches in diameter by 6 inches high. A view of the interior of this chamber is shown in Figure 4. The interior is polished to an 8 microinch finish, in order to reduce outgassing. All welds are heliarc welds, made on the interior portion of the chamber and machined. All electrode structures are mounted on an experiment plate, which is in turn suspended from the top cover of the chamber. This arrangement facilitates alignment and modification of the apparatus.

No organic materials are used inside the vacuum chamber. The vast majority of the metallic structures are made of type 304 stainless steel, with a small amount of nickel,

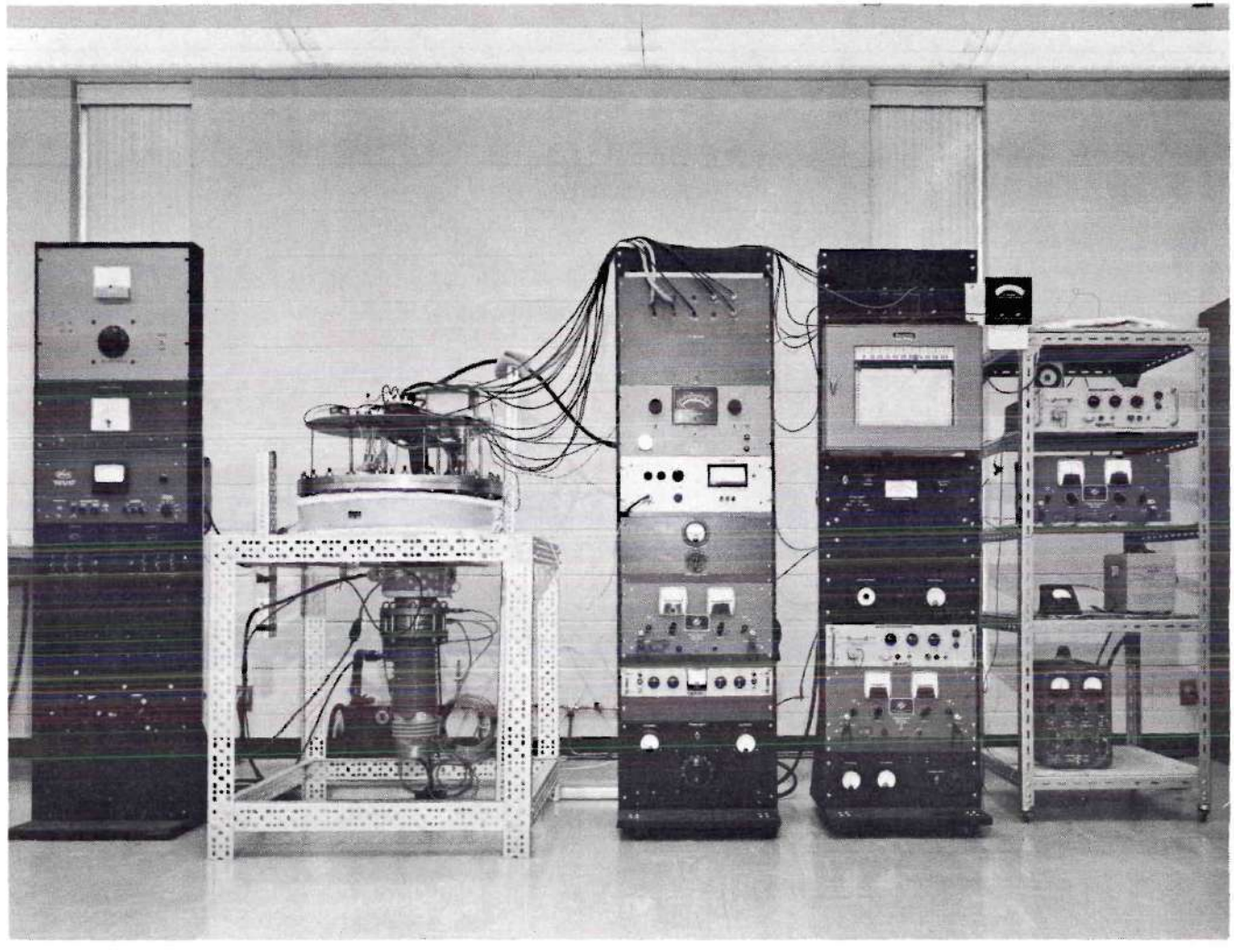

Figure 3. Overall View of the Experimental Apparatus.

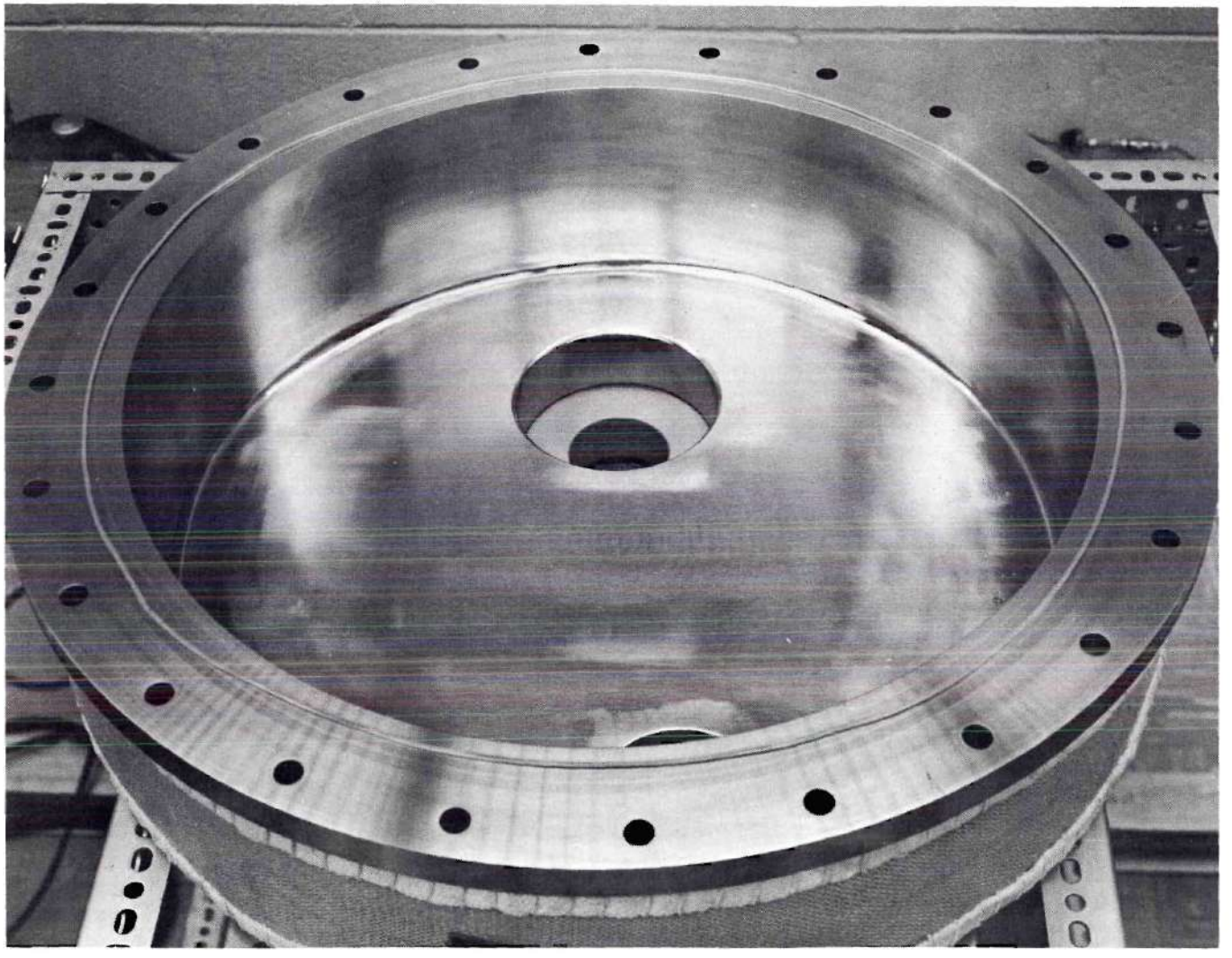

Figure 4. Interior View of the Ultrahigh Vacuum Chamber.

platinum and copper also used. All insulators are made either of alumina or steatite. All bolts extending into blind tapped holes are slotted to reduce the pumping impedance seen by entrapped regions.

Gaskets

The vacuum seals are all metal junctions of the flat type, in which a soft aluminum wire is compressed between two flat surfaces. The gasket design is similar to that utilized by Consolidated Vacuum Corporation and discussed by Holland[19] and coworkers[20,21,22] at Edwards High Vacuum, Limited. The flange surfaces should be quite flat and smooth; a typical flange surface is flat to $\pm$ .0005 inch with a 20 microinch finish. These tolerances can be achieved with surface grinding techniques. The aluminum gaskets are bakable to at least 250 ^{o}C before bonding of the gasket material to the stainless steel flanges takes place. In this work, flange temperatures are kept below 250 ^{o}C; redressing of the flange surfaces has never been required. If the aluminum gasket were to be replaced with a gold gasket, however, the resultant seal would be bakable to at least 450^{o}C without major difficulties.

The gasket material is .086 inch diameter, cold finished aluminum wire, alloy AA1100-O. The gasket is formed by butt fusing the ends of an appropriate length of this wire together. This task can best be accomplished with a small torch, while using aluminum welding flux to prevent oxidation

of the aluminum. The torch flame should be slightly reducing, and the hottest region of the flame should be confined to a region close to the junction. The most satisfactory flux employed has been the Air Reduction Company Formula Number 40 Aluminum Welding Flux; the powder flux should be mixed with methanol to form a thin paste prior to application. A small amount of compression is required at the joint in order to provide an excess of aluminum to fill in vacancies at the junction; the compression required is best determined by experimentation. With a little practice the joining technique is quite straightforward. The remaining flux is now removed from the gasket by rinsing it in hot water; the gasket is finally dressed with very fine steel wool, and cleaned with methanol just prior to use.

The mechanical details of this gasketing technique are perhaps best seen by an example. The top cover for the chamber and the corresponding flange on the vacuum chamber are 26 inches in diameter and one inch thick, and are constructed from type 304 stainless steel. The inside diameter of the chamber is 21 inches. Twenty-four bolt holes are equally spaced on a 24 1/2 in. diameter bolt circle. The diameter of the aluminum gasket is 22 inches. Silicon bronze bolts, 3/8 - 16 x 2 1/2 in. are employed for the sealing. The bolts are tightened in diametrically opposite pairs, taking care to keep the flange loading as nearly uniform as possible. All bolts are first torqued to 10 pounds-feet, followed by torqueing sequences at 20 and 30 pounds-feet. Two

to three rounds of torqueing at 30 pounds-feet are necessary before relaxation of the bolts ceases. A lubricant such as lead plate is used on the bolts to help keep the loading uniform. The load on the flange is quite substantial; a noticeable deflection is present in the one-inch-thick top cover.

Properly made, such a joint is leak free and trouble free. The top cover gasket seal described above has been made and baked over sixty times without the appearance of a detectable leak. This flange has not been baked to temperatures above 150 ^{o}C; in this temperature range, however, no evidence of gasket adherence to the flange has been found. The sealing surfaces have required no redressing during this period. The reliability and simplicity of this type of seal seem to make it ideally suited for vacuum systems requiring modest bakeout.

Pumping Apparatus

The pumping system consists of a four inch oil diffusion pump, Consolidated Vacuum Corporation type PMCU-721, followed by a water cooled chevron baffle, type BCRU-40, and a zeolite molecular sieve trap, type TSMU-40. No cryogenic trapping is employed in the vacuum system. The baffle and trap are highly effective in reducing backstreaming. Following the diffusion pump manufacturer's recommendation, the oil in the Welch Model 1402B roughing pump was drained, and replaced with Convoil 20, the same fluid which is used in the diffusion pump. This step eliminates concern over

oil from the roughing pump migrating back into the diffusion pump. No difficulties have been encountered with this arrangement.

Aluminum gaskets are utilized throughout the pumping system, except at the trap-chamber junction. The trap-chamber junction reaches a higher temperature than any other seal during bakeout; it was advisable to use a gold gasket here for this reason. All of the gaskets have proved to be completely reliable.

The oxide cathode in an electron source is very sensitive to hydrocarbon contamination, and thus provides a ready check on backstreaming of diffusion pump fluid. In order to prevent cathode contamination, it was found advisable to replace the zeolite charge in the molecular sieve trap every second pumpdown. The zeolite charge can be readily changed in the Consolidated Vacuum pumping unit. The accessibility of the zeolite charge for replacement purposes is a valuable feature of the Consolidated Vacuum sorbent trap.

Bakeout and Vacuum System Performance

The zeolite trap and vacuum chamber are baked by means of heating mantles made by the Glascol Apparatus Company. These mantles can be produced in a wide variety of shapes and power ratings. The chamber mantle, which directly heats only the cylindrical outer wall of the vacuum chamber, is partially visible in Figure 4. Insulation has been provided for the top cover of the chamber; it has proved

unnecessary to insulate the bottom of the chamber, since heat conduction from the zeolite trap during bakeout provides an additional source of heat for this region.

A bakeout generally lasts for 24 hours after the system has come to bakeout temperature. The chamber and trap walls are heated to 170 °C and 370 °C respectively. At this wall temperature all aluminum gaskets are below 150 °C. Higher bakeout temperatures are possible, but they have proved to be unnecessary. It is essential that all structures be at as high a temperature during bakeout as they will ever operate, for, if a structure is heated above its bakeout temperature following the bakeout, it will represent a large source of outgassing. This requirement means that all filaments must be at their operating temperature for a substantial portion of the bakeout cycle.

Upon reaching room temperature following bakeout the pressure indicated by a Bayard-Alpert gauge is approximately 3×10^{-9} Torr (N_2 calibration) with all sources hot, but no beams present. With a two milliampere electron beam, and an ion beam of a few tenths of a microampere, the indicated pressure is $1 - 2 \times 10^{-8}$ Torr. No significant deterioration in this performance is evident over a period of at least one month.

With all filaments cold, the indicated pressure is less than 1.5×10^{-9} Torr. This pressure is about the same as that which had been attained by the vacuum system before

any of the experimental apparatus was placed in the chamber. The addition of the experimental apparatus represented a large increase in the surface area inside the vacuum system. It thus appears that in this apparatus it is not necessary to attempt to hold scrupulously the surface area to a minimum.

Ion Beam Source and Optics

The source of lithium ions is a thermionic source of planar construction. The desired focusing characteristics are obtained through collimation and small deflection voltages. In the next two sections the characteristics of the thermionic emitter will be discussed, and the ion source and optics will be described.

Emitting Material

The emission of positive ions from hot filaments has been a well known phenomenon for many years; the subject was discussed at length by Richardson[23] in 1916. It was found that the alumino-silicates of the alkalies are among the best ion emitters at moderate temperatures (1000 ^{o}C). Blewett and Jones[24] investigated the ternary system $Li_2O \cdot X\,Al_2O_3 \cdot Y\,SiO_2$ and found that the most copious emitter was the combination $Li_2O \cdot Al_2O_3 \cdot 2Si_2O_2$. This compound bears the mineralogical name β-eucryptite. Lithium ion current densities of up to 1 ma/cm^2 are available from β-eucryptite upon heating to 1100 ^{o}C. This compound can be prepared synthetically to achieve greater purity of the emitted ions; details of the synthetic preparation are given by Allison and Kamegai.[25]

For the present crossed beam experiment, it is desirable to use an ion source which is free from contamination of other alkali ions. An appreciable sodium or potassium ion contamination of the ion beam cannot be tolerated, as the cross sections for electron impact ionization of these ions are ten to twenty times larger than the corresponding electron impact cross sections for lithium ions. Thus a one per cent potassium impurity in the ion beam could result in a twenty per cent error in the Li^+ ionization cross section. The presence of Na^+ or K^+ contaminants would require mass analysis of the ion beam prior to crossing the electron beam.

Beam purity considerations dictated the selection of synthetic β-eucryptite. Furthermore, in order to obtain an unambiguous ion velocity (See Equation (1).), it was decided to prepare the β-eucryptite from lithium compounds enriched in the mass seven isotope. This material was prepared at the Oak Ridge National Laboratories by Dr. R. A. Strehlow, to whom gratitude is expressed. All further comments refer to this isotopically purified emitter.

The β-eucryptite is prepared for use by being ground to 200 mesh size using a mullite mortar and pestle. Methanol is added to the powder to form a thin paste, and the resulting mixture is painted onto a filament of 80 mesh platinum gauze 1/8 inch wide by 1 inch long. The filament is heated in air to a temperature sufficiently high (1350 °C brightness temperature) that the β-eucryptite melts and

forms a clear glass. This process may need to be repeated several times in order to obtain a uniform coating. The resultant filament is structurally stable and ready for use.

Since it was not possible to view the ion source filament once the source was placed inside the ultrahigh vacuum enclosure, it was necessary to use the ion source filament current as a measure of the filament temperature. The temperature-current characteristics of each ion source filament were determined in an auxiliary vacuum system having a viewing port, prior to installation in the ultrahigh vacuum chamber. A Pyrometer Instrument Company Model 95 Micro-Optical Pyrometer was employed for this purpose.

Mass spectrographic analyses were made of the ion emission from the isotopically purified β-eucryptite. Upon initial heating to 1000 ^{o}C, it was found that 98 per cent of the total emission consisted of sodium and potassium ions, the latter comprising 60 per cent of the total. This large contamination is a transient phenomenon, since after approximately 5 hours of operation at 1000 ^{o}C, lithium ions constitute more than 99.9 per cent of the total emission. Moreover, the mass 7 lithium isotope represented 99.7 per cent of the total lithium emission. It was found that this source, operating at 1000 ^{o}C and having an emitting area of approximately 0.5 cm^{2}, could be relied upon to deliver ten microamperes for at least one hundred hours. Source failures were generally a result of filament burnout, rather

than depletion of the emitting material. Since source lifetime was quite adequate for this experiment, no attempt was made to optimize this parameter. The purity of the emitted ion beam obviated the necessity for including mass analysis within the experimental apparatus.

Ion Source and Optics

The ion source is of planar construction, and produces a rectangular ion beam 1/4 inch x 1/32 inch in cross section. The general configuration and typical electrode voltages are indicated in Figure 2. Beam definition in the 1/32 inch dimension is obtained primarily by means of collimation. A pair of vertical deflection and focusing plates are located as shown in Figure 2. The plates extend 1 inch along the beam flight path and are separated by 3/8 inch. The voltage applied to these plates is kept sufficiently low that the ion beam deflection is less than 2 degrees. The vertical focusing structure enables adjustment of the ion beam such that losses from the beam may be held to a negligible quantity (less than 1/2 per cent). This feature is essential, if one wishes to obtain meaningful results in this experiment. The vertical deflection feature enables important checks to be made on the accuracy of beam profile determination. It is possible to make changes in the ion beam shape and location relative to the electron beam, so that the form factor F can be varied while all other parameters are kept constant. It is imperative that the apparatus be adjusted such that the measured cross

sections are independent of modest changes in the form factor F introduced in this manner.

The horizontal deflector plates were introduced to eliminate a different problem. It was found that the Li^{+} beam contained a small component, about one part in 10^{8}, which had either lost energy or been charge-stripped in collisions with the knife edges of the collimating slits in the ion source. Some of these ions can travel directly into the Li^{++} detector, when the ion source geometry is linear. If, however, a small deviation in the ion beam is introduced electrostatically, then that portion of this component which had previously entered into the Li^{++} detector now suffers twice as much deflection as the main beam. The horizontal deflector introduces an 8 degree bend in the main ion beam, following the last slit edge that the ion beam is allowed to strike. The bend is sufficient to prevent the unwanted component from entering the post-interaction analyzer, and thus eliminates this cause of stray current to the Li^{++} detector.

A photograph of the ion source and associated structures is shown in Figure 5. The important sections of the source are labeled, and a length scale is shown. The ion source is capable of delivering 1.5 μa of well focused lithium ions at 1 keV energy. For this experiment the source is generally operated near 2×10^{-7} amperes to provide a lower pressure and longer lifetime. As expected, no

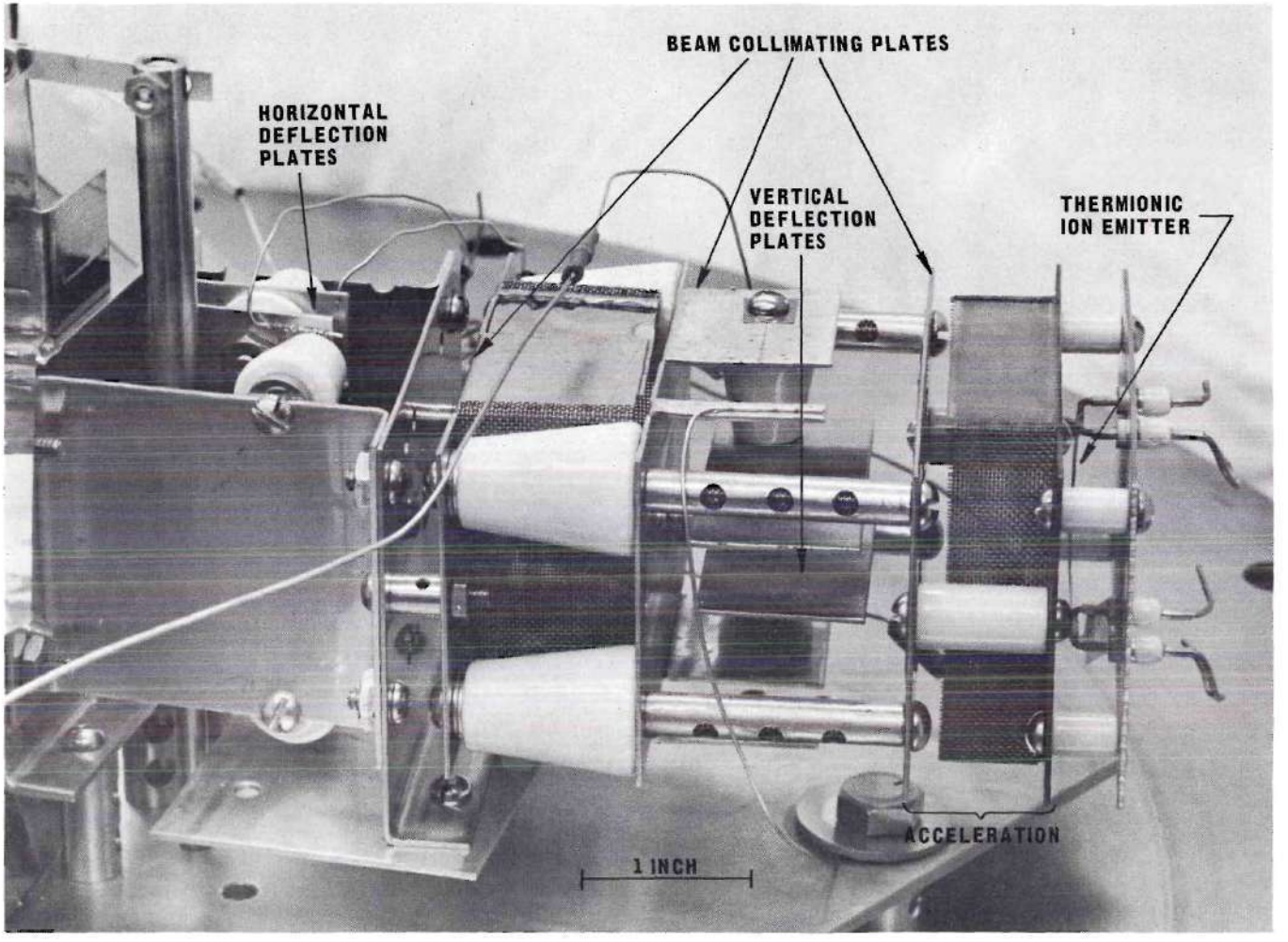

Figure 5. Thermionic Ion Source, Collimation and Deflection Structures.

evidence has been observed which suggests the production by the thermionic source of any ions in excited states.

Interaction Region

The interaction region is designed to provide a field free space for intersection of the ion and electron beams. The interaction region is defined by a T shaped bracket, to which the ion and electron sources are secured, and on which the movable slit scanner rides. A photograph of this region is shown in Figure 6, looking toward the sources of ions and electrons. In the view, the slit scanner is positioned so as to allow the beams to pass through the interaction region without obstruction. The slit scanner should intercept the ion and electron beams as close to the interaction region as is feasible; the scanner shown here intercepts the two beams approximately 3/8 inch prior to their intersection. It may be noticed in the photograph that two pairs of slits are present on the scanner. One set has a slit height of .020 in., while the other set is .009 in. high. This arrangement permits the determination of beam profiles with two significantly different slit sizes. If the beams are highly nonuniform, the smaller slit system might show up fine structure in the beam profiles which was not seen using the larger slits. This refinement proved to be unnecessary, and only the .020 inch slits were employed in the majority of the measurements.

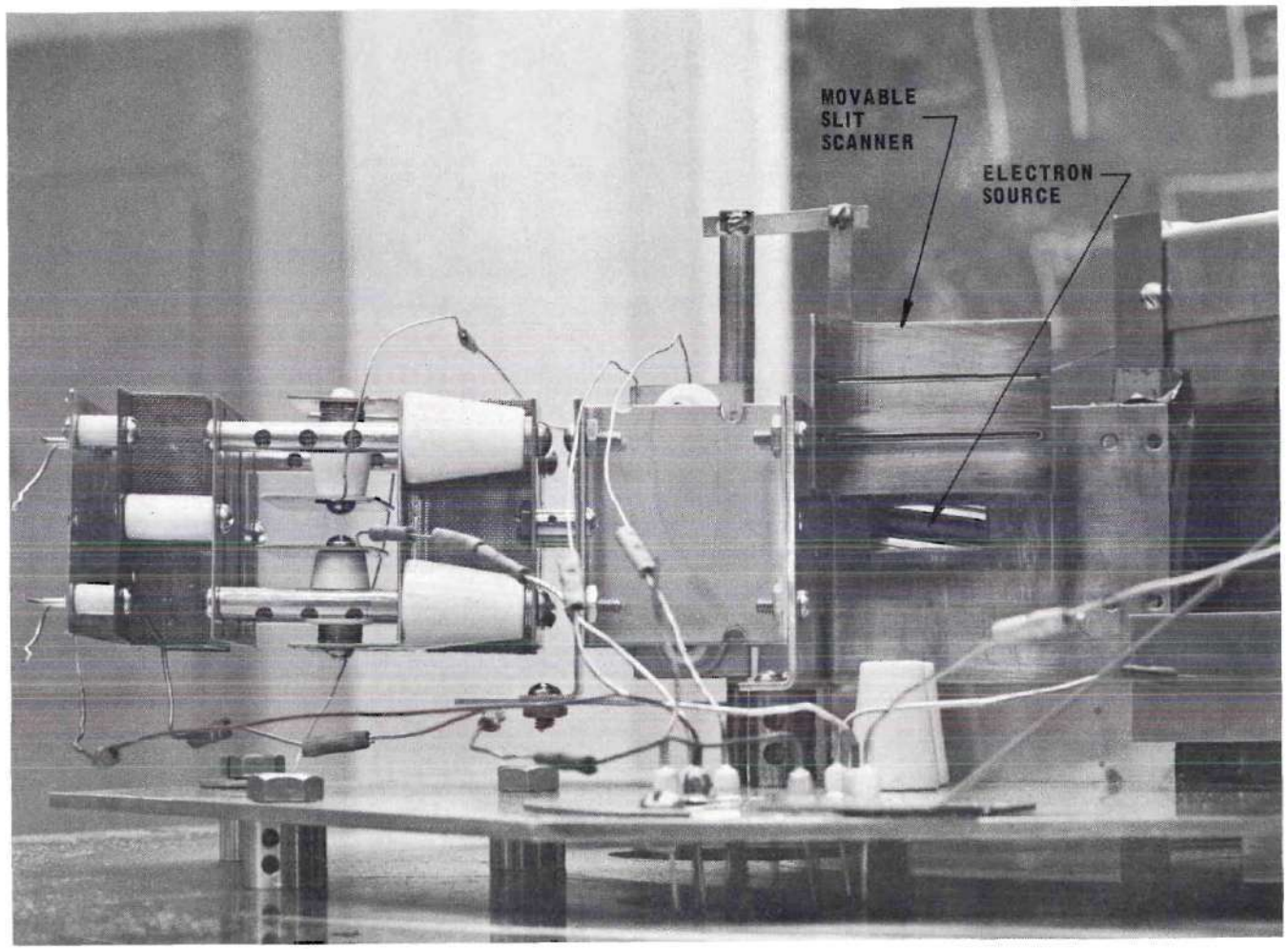

Figure 6. Interaction Region Seen from the Location of the Electron Beam Faraday Cup.

The linear motion of the slit scanner is introduced by means of a metal bellows assembly positioned with a micrometer drive. The bellows itself was manufactured by the Metal Bellows Corporation; constructional details of the scanner drive assembly are available from the author upon request.

Electrostatic Analyzer

Following transit through the electron beam, the ion beam, which now contains Li^{+} and Li^{++} ions traveling at the same velocity, must be separated into its various charge states. Since the Li^{++} component may be 10^{-9} times the size of the Li^{+} beam, the separation must be performed very carefully in order to prevent stray particles from the Li^{+} component from obscuring the Li^{++} component. It is desirable to analyze the ion beam in as close a proximity to the interaction region as possible; the analyzer fields, however, must not penetrate into the beam interaction region. Either electrostatic or magnetostatic analyzers could be used to effect this separation. For this application the electrostatic analyzer was considered superior to the magnetostatic analyzer, both from space considerations and the fact that the fringe fields of the electrostatic analyzer are more easily controllable.

Charge state separation is accomplished by an inclined parallel plate electrostatic analyzer, as shown in Figure 2. The structure is a modification of an energy selector proposed

by Yarnold and Bolton[26], and elaborated upon by Harrower[27]. The ion beam enters the analyzer at an angle of 45 degrees with respect to the plates. The singly and doubly charged ionic species are separated in the electric field of the analyzer and exit at angles of 45 degrees into their respective Faraday cups. If the incident ionic beam is composed of projectiles occupying a small angular region $\Delta\theta$ about θ=45 degrees, then, to first order in $\Delta\theta$, both components of the beam are focused on their respective exit apertures. This angular refocusing, plus the ability to produce large deflections in a small physical space, represent major advantages over the more conventional parallel plate electrostatic energy analyzer.

The plates of the analyzer are separated by 1 5/16 in., while the spacing between adjacent apertures in the grounded plate of the analyzer is 2.0 inches. The aperture sizes are approximately 3/8 in. x 3/4 in.; the size is thus much greater than the nominal 1/16 in. x 1/4 in. size of the ion beam in this region. The analyzer plates are sufficiently large (5 inches x 9 inches) that end field effects are well removed from the vicinity of the ion beams.

The baffle plate in the analyzer (See Figure 2.) is held at the value of the local equipotential and does not seriously disturb the uniform electric field of the analyzer. The use of this plate was necessary as a consequence of the very large difference in magnitude between the Li^{+} and Li^{++} currents. The need for this plate arose as follows. As the

Li^+ beam traverses the vacuum chamber, the following interactions with the residual gas are among those possible:

$$\begin{aligned} &\text{Ionization:} && Li^+ + R \rightarrow Li^+ + R^+ + e \\ &\text{Charge Transfer:} && Li^+ + R \rightarrow Li + R^+ \end{aligned} \qquad (6)$$

where R is a residual gas molecule. In either case the R^+ ion formed will be a relatively slow ion. The Li^+ beam thus produces a line of slow ions along its flight path. When this process occurs within the analyzer, the slow ions are accelerated toward the grounded plate of the analyzer. Those ions formed directly above the Li^{++} beam opening are accelerated into the Li^{++} cup region. Consideration of the chamber pressure (10^{-8} Torr) and typical cross sections[28,29] for these processes shows that the ions so entering the Li^{++} beam opening are considerably more numerous than the expected signal current of Li^{++} ions. The baffle plate intercepts these ions before they reach the Li^{++} beam opening, and thus eliminates this problem. The baffle plate is sufficiently small that neither beam comes closer than 3/8 inch to it. When this problem first arose, the Li^{++} cup was situated very close to the grounded analyzer plate, much as the Li^+ cup is positioned in Figure 2. At that time the baffle plate was absolutely essential; since then, however, the Li^{++} cup has been moved back to the position indicated in the figure. It is likely that the baffle plate is now much less essential.

It should also be noted that while reactions (6) can mask the Li^{++} beam, they represent a completely negligible attenuation of the Li^{+} beam.

In spite of the large openings into the analyzer, it performs very nearly as predicted under the assumptions of infinitely large parallel planes with vanishingly small entrance and exit apertures. Performance tests show that there is a broad plateau of analyzer voltage over which both components of the ion beam suffer no losses in traversing the analyzer to their appropriate exit apertures. The baffle plate voltage adjustment has been shown to be noncritical. Wide variations of the baffle plate voltage with respect to the total analyzer voltage do not impair the performance of the analyzer.

Ion Collection and Current Measurement Systems

The design and operation of the Li^{+} measurement system is routine and presents few problems. The magnitude of the Li^{++} beam current, about 10^{-15} amperes, requires that special precautions be taken, and special techniques be employed, if meaningful measurements are to be made. The next two sections discuss the collection and measurement systems for these two ion beam components.

Li^{+} Collection and Measurement System

As seen in Figure 2, the Li^{+} Faraday cup is a deep cup with the surface being struck by the ion beam inclined

with respect to the beam. The solid angle subtended by the entrance to the cup at the region where the ion beam strikes the cup is less than one per cent of the total solid angle. In addition, secondary electron and reflected ion suppression structures are incorporated into the cup, but it has been demonstrated that the cup is essentially 100 per cent efficient in retaining secondary charged particles even when no voltages are applied to the suppression structures. While reflected Li^+ ions did not impair the performance of this collector due to the geometry employed, it must be noted that energetic reflected Li^+ ions are present in appreciable numbers. Brunée[30] finds a reflection coefficient of 0.16 for 1 keV Li^+ ions incident on clean molybdenum surfaces; he further finds that the energy distribution of these reflected ions is essentially flat out almost to the primary ion energy. Thus energetic reflected ions are a phenomenon which must be considered throughout the entire ion beam flight path.

The Li^+ beam current is measured with a Keithley Model 610R electrometer. The instrument calibration is frequently checked with a Gyra Model CS-57 current source. The accuracy of the Li^+ current instrumentation is better than $\pm$ 2 per cent.

Li^{++} Collection and Measurement System

The Li^{++} Faraday cup, as seen in Figure 2, sits back from the analyzer, but its entrance aperture is still large with respect to the ion beam size. The Li^{++} aperture serves to suppress secondary electrons from the Li^{++} cup, and to

prevent slow electrons from passing through the analyzer to the Li^{++} cup. It should be noted that a slow electron can be attracted into the analyzer entrance, be accelerated to the analyzer high voltage plate, and, if the electron is elastically reflected at the plate, be energetically capable of traversing the analyzer to the Li^{++} cup. Since operation of the electron source tends to fill the vacuum chamber with a "cold" electron gas, this source of stray current to the Li^{++} cup was a serious problem until the Li^{++} aperture was installed. It has been shown that this Faraday cup collects the Li^{++} beam component with essentially 100 per cent efficiency. The 100 per cent collection efficiency is demonstrated in the following manner. The magnitude of the Li^{++} beam component is too small and too masked in noise to permit a direct observation of small changes in this current, while suppression voltages are being varied. Consequently, it was necessary to investigate the collection efficiency by indirect methods. The electrostatic analyzer voltage was doubled, thereby deflecting the Li^{+} beam into the Li^{++} cup. Variation of suppression voltages could now easily show that the Li^{++} cup collected the Li^{+} beam with essentially 100 per cent efficiency. There is, however, a possibility that the Li^{++} beam might not be collected with the same efficiency as the Li^{+} beam. In order to investigate this point, the ionization cross section at a fixed electron energy was measured as a function of the electrostatic

analyzer voltage. There exists a wide plateau of this voltage over which the measured cross sections do not change detectably. Since the Li^{++} beam collection geometry changes appreciably as the Li^{++} beam is swept across the Li^{++} cup, and since the measured cross sections do not change appreciably in this process, it is very unlikely that the Li^{++} beam collection efficiency is less than 100 per cent. This observation, coupled with the demonstrated 100 per cent collection efficiency for Li^{+} ions, leads to the conclusion that the Li^{++} collection structure is essentially 100 per cent efficient.

The magnitude of the Li^{++} current requires that the cup and its lead wire be carefully shielded from stray charged particles. The Li^{++} aperture, Faraday cup, and its lead are completely enclosed with the exception of the exit aperture of the analyzer through which the Li^{++} beam travels. In the 10^{-15} ampere range all insulators must be considered as possible sources of leakage and spurious currents. Thus, for the steatite insulator which supports the Li^{++} aperture, the following requirements were found:

(1) The insulator must be mechanically secured to a grounded structure, rather than the Li^{++} cup.

(2) The insulator must be electrostatically shielded from the Li^{++} cup.

Requirement (1) is readily seen from an estimate of the leakage current across the insulator upon application of a 100 volt potential. The second requirement arises from the fact

that, upon application of a potential across the insulator, transient currents with a time constant of hours flow through the insulator. These currents produce a time varying electric field which can in turn induce a time varying charge on the Li^{++} cup. The net result is a varying current to the Li^{++} cup with a time constant of hours. Electrostatic shielding of the insulator from the Li^{++} cup and its lead wire eliminates this effect.

The current to the Li^{++} cup is measured with a Cary Model 31 Vibrating Reed Electrometer. The electrometer preamplifier head mounts directly above the Li^{++} cup vacuum feedthrough connector. Since the vibrating reed electrometer is a high input impedance device, care must be exercised to keep the Faraday cup and its electrical lead carefully insulated from ground. Only high quality alumina and sapphire insulators are allowed to touch the Li^{++} cup and its lead. In this manner the leakage resistance from the cup to ground has been kept greater than 5×10^{13} ohms, as indicated by a Keithley Model 610R Electrometer. The output of the vibrating reed electrometer is fed into a 10 inch Honeywell Electronik Model 15 potentiometric recorder with an accuracy of 0.25 per cent.

Two modes are available for measuring currents with the vibrating reed electrometer. In the first mode, the instrument measures the voltage drop produced by the unknown current across a known large resistance. This mode has the

advantages of simplicity and direct readout of the magnitude of the ion current, but, as will be seen subsequently, these advantages accrue at the expense of additional noise and reduced accuracy. In the second mode of operation, known as the rate-of-charge mode, the instrument indicates the instantaneous voltage developed across a known precision capacitor by the beam current. If the beam current is constant, then

$$I = \frac{\Delta Q}{\Delta t} = \frac{\Delta V}{\Delta t} C \qquad (7)$$

where C is the capacitance of the capacitor being charged by the current I, and Δt is the time interval over which the voltage changed by ΔV volts. The beam current is thus determined by measuring the average time derivative of the output voltage of the vibrating reed electrometer, and multiplying by the capacitance of the precision capacitor. This method requires the use of a recorder, and a considerable amount of additional time is required in order to determine the magnitude of the ion current, but, for measurements below 10^{-13} amperes, the improved accuracy completely justifies the additional effort and time involved in the rate-of-charge measurement.

The vast improvement gained by rate-of-charge measurements is best shown by an example. Figure 7 shows two determinations of the same current, one made using a 10^{12} ohm-resistor, and the other made using the rate-of-charge mode. In both cases the dashed lines represent a ± 5 per cent deviation from the mean. It is quite apparent that the rate-of-charge mode produces a more accurate measurement of this current in a given time interval. The rate-of-charge mode permits routine slope determinations

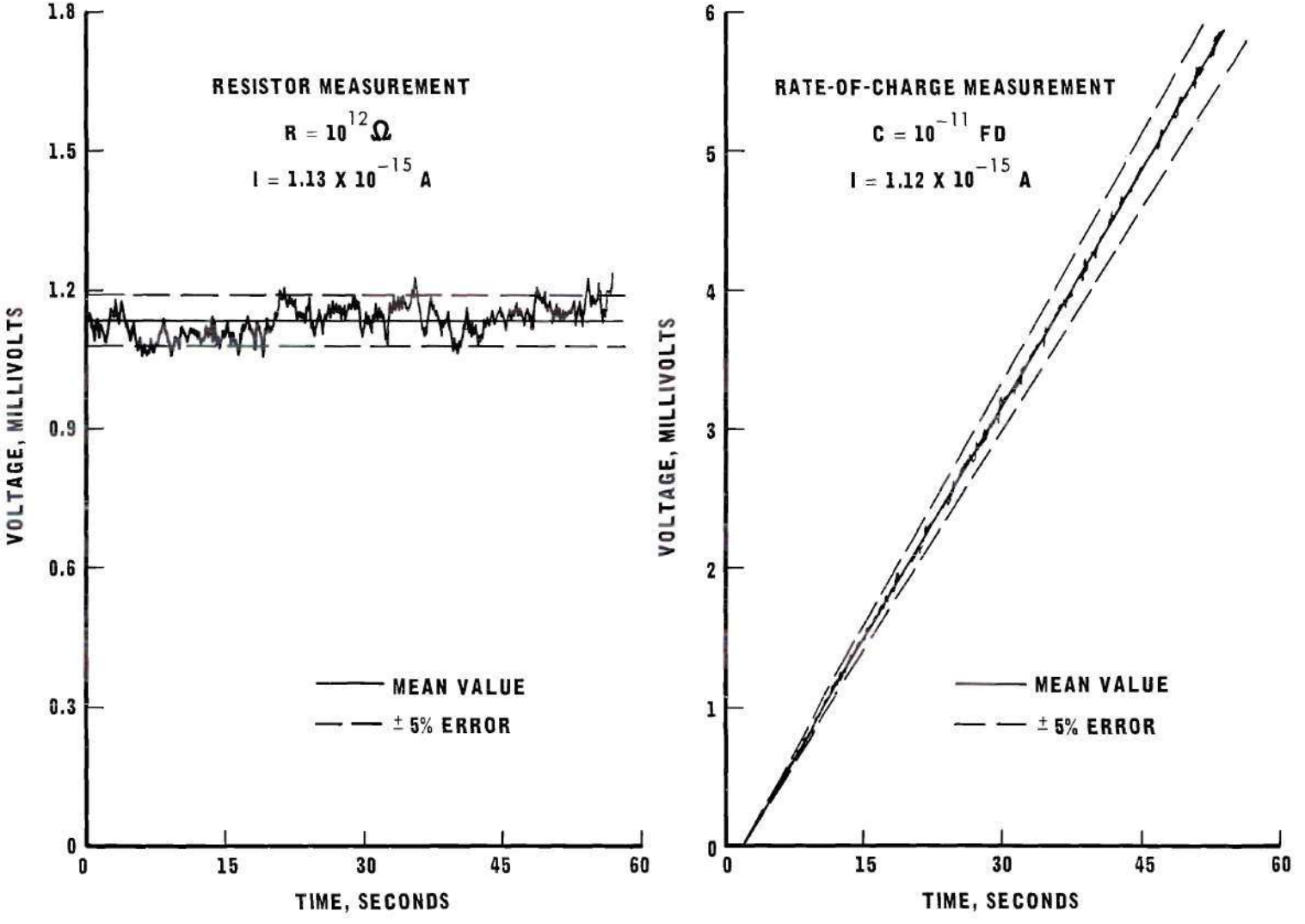

Figure 7. Typical Rate-of-Charge and Resistor Current Measurements with a Vibrating Reed Electrometer.

to ± 1.0 per cent accuracy, a very difficult if not impossible accuracy to achieve using the resistor method. The rate-of-charge mode of operation was accordingly adopted for all Li^{++} detector current measurements. Equation (7) shows that the accuracy of the rate-of-charge measurement depends upon the accuracy with which the capacitance of the charging capacitor is known. This capacitance was determined by measuring a known current from a Gyra Model CS-57 current source in the rate-of-charge mode; the resulting capacitance was $1.00 \pm .03 \times 10^{-11}$ farads. Since the accuracy with which the voltage derivative can be determined is usually better than 1 per cent, an overall error of ± 3 per cent in the determination of currents to the Li^{++} cup is indicated.

Electron Source, Collection and Measurement Systems

The electron source is a modified 6L6GC beam power tube. A beam power tube was chosen for the source since it is designed to produce an approximately rectangular electron beam. The 6L6GC is prepared for use in the following manner. The tube basing and envelope are removed*, and the plate structure is cut back, exposing the cathode and grids. The remaining plate sections are bent into a position for spot welding to a mounting bracket. This adjustable bracket is then properly positioned with respect to the ion beam. The mounted electron source can be seen in Figure 6.

---

*Operational and cathode activation procedures for oxide cathodes in demountable vacuum systems are discussed in Appendix III.

It may be noted in this view that the electron source is slightly canted; this cant is deliberately introduced to make the electron beam extend over a greater distance in the z-direction. Earlier versions were not canted, and it was found that, as a result of the highly peaked nature of the electron beam profile, the form factor F was not satisfactory with respect to the criteria developed in Chapter II. Even with this cant the electron beam is still well contained within the ion beam. The electrons are accelerated from the negative cathode to ground potential. The screen grid is normally set at ground potential, and the control grid is employed to adjust the electron beam intensity.

The electron Faraday cup is similar in design to the Li^+ Faraday cup. It also efficiently retains secondary electrons with no suppression voltages applied. An aperture plate is placed in front of the electron cup; its design is such as to allow only electrons which have passed through the ion beam to enter the electron Faraday cup. During data collection, the current to this plate is always less than 0.5 per cent of the total electron beam current.

The electron current is determined by measuring the voltage drop produced by the electron beam across a precision resistor. A General Electric self-balancing potentiometer is employed for this purpose. The estimated error of electron current determination is $\pm$ 1.0 per cent. The electron energy is set with a John Fluke Model 413 D power supply,

whose accuracy is $\pm$ 0.25 per cent for voltages which are multiples of 10 volts. The approximate energy distribution of the electron beam was determined by retarding potential techniques; the electron beam energy distribution has a halfwidth of approximately 2 eV, centered approximately 3 eV below the accelerating voltage indicated by the John Fluke power supply.

Shielding and Stray Current Reduction

The necessity for reducing stray currents to the Li^{++} detector to the lowest possible level has already been pointed out. Steps taken in this direction which have been previously mentioned include the use of the horizontal deflector, the analyzer baffle plate, and the Li^{++} aperture plate, and the complete shielding of the Li^{++} detection system. In addition to these measures it was necessary to enclose the electron source, and to provide baffling against particles entering the electrostatic analyzer through its sides or top. These steps reduced the stray electron current to the Li^{++} detector to a low but not negligible level. Further reduction in this stray electron current is achieved by means of external magnets located above the Li^{++} detection region. This magnetic field acts as a partial shield against electrons entering several small holes in the Li^{++} detector shielding structure. Properly located, these magnets produce a negligible field in the vicinity of the electron beam. That this externally produced magnetic field does

not impair the performance of the experimental apparatus is assured through frequent checks, as discussed in Chapter IV.

CHAPTER IV

EXPERIMENTAL PROCEDURES AND RESULTS

An important segment of the experimental procedure is concerned with obtaining the correct Li^{++} electron ionization signal from the several currents measured at the Li^{++} detector. This matter is considered first, followed by discussions of the measurement procedures, checks for consistency, and the experimental results and probable errors.

Currents to Li^{++} Detector

Currents measured at the Li^{++} detector include components produced by the spurious collection of Li^{+} ions and electrons from the two crossed beams; by charge-stripping and electron-impact ionization of the Li^{+} beam; and by contact and thermal potentials present in the Li^{++} detector assembly. Several terms must be defined in order to describe these components concisely. The following definitions are employed.

(1) $I^{++}_{sig}(I,e)$ is that current of electron-impact-produced Li^{++} ions present when an ion beam of I amperes and an electron beam of e amperes are present in the interaction region.

(2) $I^{++}(I,e)$ is that current measured at the Li^{++} detector with a Li^{+} beam of I amperes and an electron beam

of e amperes present.

(3) $I^{++}(I,0)$ is that current measured at the Li^{++} detector with only a Li^{+} beam of I amperes present.

(4) $I^{++}(0,e)$ is that current measured at the Li^{++} detector with only an electron beam of e amperes present.

(5) $I^{++}(0,0)$ is the small background current measured at the Li^{++} detector with no beams present. This current is a leakage current driven by thermal and contact potentials.

Several assumptions are now made regarding these currents; if these assumptions be valid then it becomes possible to extract $I^{++}_{sig}(I,e)$ from the other I^{++} currents above. After statement of these assumptions, and deduction of the resultant expression for the Li^{++} electron-impact-ionization component, it is necessary to show that, within the stated experimental error, these assumptions are valid in the present experimental apparatus. At this point the assumptions need no longer be called "assumptions," but rather are behavioral properties of the experimental apparatus under proper operating conditions. The assumptions are the following:

(1) $I^{++}(0,0)$ represents a steady background current whose magnitude is independent of the presence or absence of either or both of the ion and electron beams.

(2) The quantity $\left[I^{++}(I,0) - I^{++}(0,0)\right]$ represents a Li^{+} beam noise component whose magnitude is unaffected by the presence or absence of the electron beam.

(3) The quantity $\left[I^{++}(0,e) - I^{++}(0,0)\right]$ is an electron current

to the Li^{++} detector, the magnitude of which is independent of the presence or absence of the ion beam.

Under these assumptions, an expression for $I^{++}(I,e)$ may be determined as follows:

$$I^{++}(I,e) = I^{++}_{sig}(I,e) + \left[I^{++}(I,0) - I^{++}(0,0)\right] + \left[I^{++}(0,e) - I^{++}(0,0)\right] + I^{++}(0,0). \quad (8)$$

Simplifying this result and solving for I^{++}_{sig} yields

$$I^{++}_{sig}(I,e) = \left[I^{++}(I,e) - I^{++}(I,0)\right] - \left[I^{++}(0,e) - I^{++}(0,0)\right], \quad (9)$$

which is the desired expression for the electron-impact-ionization component. It remains to be shown, however, that the assumptions leading to Equation (9) are valid.

At an electron energy below the second ionization threshold (75.6 eV), the quantity $I^{++}_{sig}(I,e)$ should be zero. The measured value can be nonzero for several reasons, including

(1) the contamination of the Li^{+} beam with K^{+} and/or Na^{+} impurities (Chapter II);

(2) the presence of Li^{+} ions in excited states (Chapter II);

(3) an increase in the collected charge-stripped Li^{++} component, as a result either of the converging influence of the electron beam space charge or of pressure

changes resulting from turning on the electron beam (Chapter II); and

(4) the non-validity of any of the three assumptions leading to Equation (9).

It has been found that $I^{++}_{sig}(I,e)$ is zero below threshold, to within two per cent of typical values of $I^{++}_{sig}(I,e)$ well above threshold. This result has been determined frequently for various electron currents, ion currents, and electron energies below threshold. The variety of conditions under which $I^{++}_{sig}(I,e)$ is zero below threshold should suffice to show that none of the four mechanisms above are operative, for it is unlikely that two errors could be self-canceling over a variety of operating conditions. Further checks are possible, however, since of all the possible mechanisms for producing a nonzero $I^{++}_{sig}(I,e)$ below threshold, only an error in the electron correction term, $\left[I^{++}(0,e) - I^{++}(0,0)\right]$, can lead to a negative value. Thus any possible cancellation of errors producing zero signal current must be associated with the electron correction term. By means of small changes in the positions of the external magnets it is possible to introduce an order of magnitude change in the electron correction term. The ionization signal current below threshold remains zero throughout such changes in the electron correction term. Thus an accidental cancellation can be effectively ruled out as a possibility. It should be finally noted that the electron correction term is not a linear function of electron

current; this fact alone makes an accidental cancellation unlikely.

In addition to the changes in the electron correction term, the measured signal current is found to be independent of changes in the magnitude of the background current, $I^{++}(0,0)$, and the ion beam noise current, $\left[I^{++}(I,0) - I^{++}(0,0)\right]$. The resulting conclusions are therefore that none of the four mechanisms discussed previously are operative, and that the three assumptions concerning the currents to the Li^{++} detector are valid.

Measurement Procedures

Before cross section measurements can be made, a number of preliminary adjustments of the apparatus are necessary. These preliminary adjustments are listed below, followed by a short explanation where necessary.

(1) Following completion of the vacuum chamber bake-out, it is necessary to wait approximately 48 hours for the background current $I^{++}(0,0)$ to decay and stabilize. Before this time, the background current is too large and insufficiently steady to permit accurate measurements; the primary sources of this current are thermal gradients, contact potentials, and stressed insulators. The remaining adjustments take place after this current has stabilized.

(2) The stray electron current to the Li^{++} detector is minimized by means of external magnets located near the detector portion of the vacuum chamber. The absence of

appreciable stray magnetic fields in the interaction region is assured by observing the electron current to the electron cup aperture plate at low electron energies (~50 eV). Since a small deflection of these electrons is sufficient to produce a significant current to the electron Faraday cup aperture plate, the absence of such current assures that the effect of the external magnets in the interaction region is small.

(3) The voltages of the electrostatic analyzer and horizontal deflector are adjusted such that both the Li^{+} and Li^{++} beams are centered on their respective exit apertures in the electrostatic analyzer. The aperture sizes are sufficiently large that ± 5 per cent changes in the electrostatic analyzer voltages do not affect either of these currents. Particle losses in the analyzer are checked by doubling the analyzer voltage, thus deflecting the Li^{+} beam into the Li^{++} detector. The electrostatic analyzer and horizontal deflector voltages are always adjusted such that the Li^{+} currents measured at these two detectors agree to within the accuracy of the measurement instrumentation.

(4) The Li^{+} beam is focused so as to restrict losses from the beam to less than 1.0 per cent. Particle losses in the 1/32 inch dimension of the ion beam have not been encountered, but their possible presence can be determined by varying the electrostatic analyzer and horizontal deflector voltages. Particle losses in the 1/4 inch (vertical)

dimension are determined by measuring the increase in ion beam intensity resulting from application of the electron beam. The increase in ion beam intensity usually saturates at a few milliamperes electron beam intensity. The ion beam loss is taken to be the fractional increase in ion beam intensity as the electron beam intensity is increased from 0 to 10 milliamperes.

(5) The ion beam profile is adjusted by means of the vertical deflection structure so as to obtain a "good" form factor.

(6) A check is made to assure that none of the currents measured at the Li^{++} detector are rapidly varying functions of analyzer voltage. Such a condition may exist if either beam passes too close to the edge of an aperture.

Since some of these adjustments are interrelated, it is necessary to recheck all of them after the initial adjustments are made, and perhaps to make some slight readjustments. On occasion it may be impossible to meet all of these requirements. For example, it has at times been impossible to obtain small Li^{+} beam losses without introducing an unacceptable ion beam profile. This condition generally necessitates disassembly of the apparatus, and replacement of the thermionic ion emitter. Once the preliminary adjustments have been satisfactorily completed, the cross section measurements can proceed. The following is the step-by-step procedure employed to obtain the

ionization cross section at a particular electron energy, electron beam intensity, and ion beam intensity.

(1) The electron energy, ion beam intensity and electron beam intensity to be utilized in the measurements are selected.

(2) The slit scanner is lowered across the beams, to provide data for calculation of the form factor F. The normal scanner increments are .020 inches.

(3) The quantities $I^{++}(I,0)$ and $I^{++}(I,e)$ are measured sequentially. Normally three measurements of each of these currents are made using the rate-of-charge mode. The length of time utilized for each determination is approximately forty seconds.

(4) The quantities $I^{++}(0,e)$ and $I^{++}(0,0)$ are measured; each current is measured at least twice.

(5) From (3) and (4), respectively, average values are calculated for $\left[I^{++}(I,e) - I^{++}(I,0)\right]$ and $\left[I^{++}(0,e) - I^{++}(0,0)\right]$. From these quantities an average $I^{++}_{sig}(I,e)$ is determined using Equation (9). The ionization cross section is then calculated by use of Equations (2) and (3).

The raw data and calculated results of a typical measurement are presented in Appendix II. The data are taken at randomly varied electron energies. In addition, the ion and electron beam intensities are periodically varied to assure that the measured cross sections are independent of these parameters. Many of the checks on performance of the

apparatus are made at 500 eV electron energy and at an electron energy below threshold. Approximately one out of every five measurements is a repetition of one of these check points; this procedure enables frequent checks to be made on the apparatus performance.

Possible Errors and Checks for Consistency

A number of checks must be made before proper operation of the apparatus is assured. The results of the checks presented here pertain to the performance of the experimental apparatus during those periods in which the experimental results can be considered valid. It should be emphasized, however, that the consistency exhibited by these checks was not obtained every time the apparatus was operated. Each of the effects discussed in Chapter II has, at one time or another, been observed in the course of the checking procedure, and has necessitated appropriate corrective measures before valid results could be obtained.

Figures 8a and 8b show the dependence of the measured cross sections on electron and ion beam intensities, respectively, at an ion beam energy of 1000 eV. The scatter in these results is well within the acceptable error of this experiment.

The measured cross section below threshold is zero, to within $\pm$ 2 per cent of the 500 eV cross section. As stated previously, this result assures the validity of the continuous beam technique utilized in this apparatus, and, as will

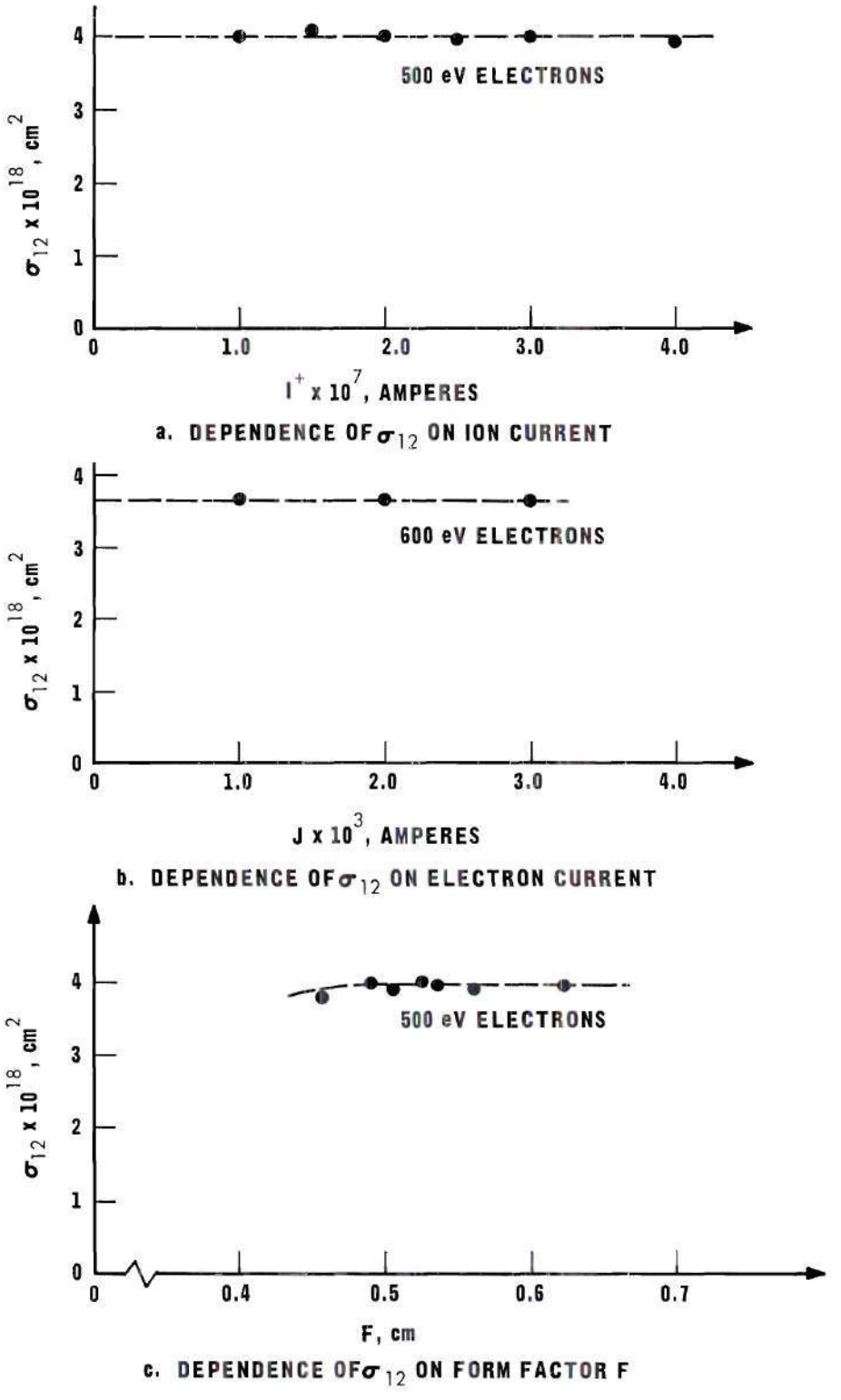

Figure 8. Dependence of the Measured Cross Sections on Various Experimental Parameters.

be shown in Appendix IV, indicates that the use of any beam modulation scheme would represent no improvement in the performance of the apparatus. In addition, this result precludes the possibilities of significant Na^+ or K^+ contamination of the Li^+ beam; of the presence of significant numbers of Li^+ ions in excited states; and of significant electron beam convergence of more widely scattered charge-stripped Li^{++} ions. Thus the zero cross section below threshold represents one of the most important single checks on the operation of the apparatus.

It is necessary that the measured cross sections be independent of some changes in the beam profiles, and hence of changes in the form factor. This check is necessary to assure that the form factor measurement does not introduce an appreciable error, as pointed out in Chapter II. Figure 8c depicts the variation of the 500 eV cross section with the form factor F, all other parameters being held constant. The ion beam is not perfectly uniform, and hence no simple interpretation can be given to F; it can be said, however, that F is some sort of measure of the "height" of the ion beam. In fact, these variations in F were introduced by varying the vertical focus voltage and hence the "height" of the ion beam.

The cross section is essentially independent of changes in the form factor F except for the rolloff seen below F = 0.47. These data were taken with electron beam

profiles which were nearly identical. The rolloff is thus a result of the ion beam becoming too small to accomodate the space charge spreading of the electron beam. Were cross section measurements made at F = 0.45 as a function of electron beam intensity, it would be found that the measured cross sections would increase as the electron beam intensity decreased. As is evident from Figure 8b, such is not the case when measurements are made with a value of F which is in the plateau portion of the curve. These facts, coupled with the observation that the 500 eV cross section is unaffected by increasing the ion beam energy from 1000 eV to 1500 eV, indicate that no serious errors are present in the form factor determination.

The measured cross sections are also shown to be independent of small changes in the electrostatic analyzer and horizontal deflector voltages. As stated previously the measured cross sections are independent of wide variations in $I^{++}(0,0)$, $I^{++}(0,e)$, and $I^{++}(I,0)$. At the highest electron energies employed, 700 eV and 800 eV, the electron source occasionally tended to arc over from the control grid to the grounded screen grid. In order to avoid this difficulty, it was necessary to operate the screen grid at -100 V when 700 eV or 800 eV electron energies were employed. There was a possibility of the screen grid electric field penetrating appreciably into the interaction region. To investigate this point, the 500 eV cross section was measured as a function of screen grid voltage over the range from 0 V

to -150 V. No detectable variation in σ_{12} was observed, and it is concluded that the use of -100 V on the screen grid at high electron energies introduces no appreciable error.

The same results have been obtained with several different ion and electron sources. Items such as the calibration of the measurement instrumentation and the efficiency of the Faraday cups have been discussed in the previous chapter.

Measurement Results and Discussion of Errors

The cross sections for single ionization of lithium ions by electron impact have been measured for electron energies over the range from below threshold to 800 eV. The results of these measurements are shown in Figure 9, while the results are presented in tabular form in Table 1.

The tabular data pertain to the actual measured cross sections, and not to the smooth curve which has been drawn as a "best fit" to the measured results. The maximum probable errors of the measurements are indicated by vertical bars on the graph, and are shown numerically in Table 1.

The systematic errors arise primarily from instrumentation calibration errors; they are estimated to be a maximum of $\pm$ 6 per cent at all electron energies. The random errors are more difficult to estimate for the following reason. Over short periods of time, repeated measurements of the cross section at 500 eV, for example, may exhibit very little scatter (less than $\pm$ 2 per cent). Over periods

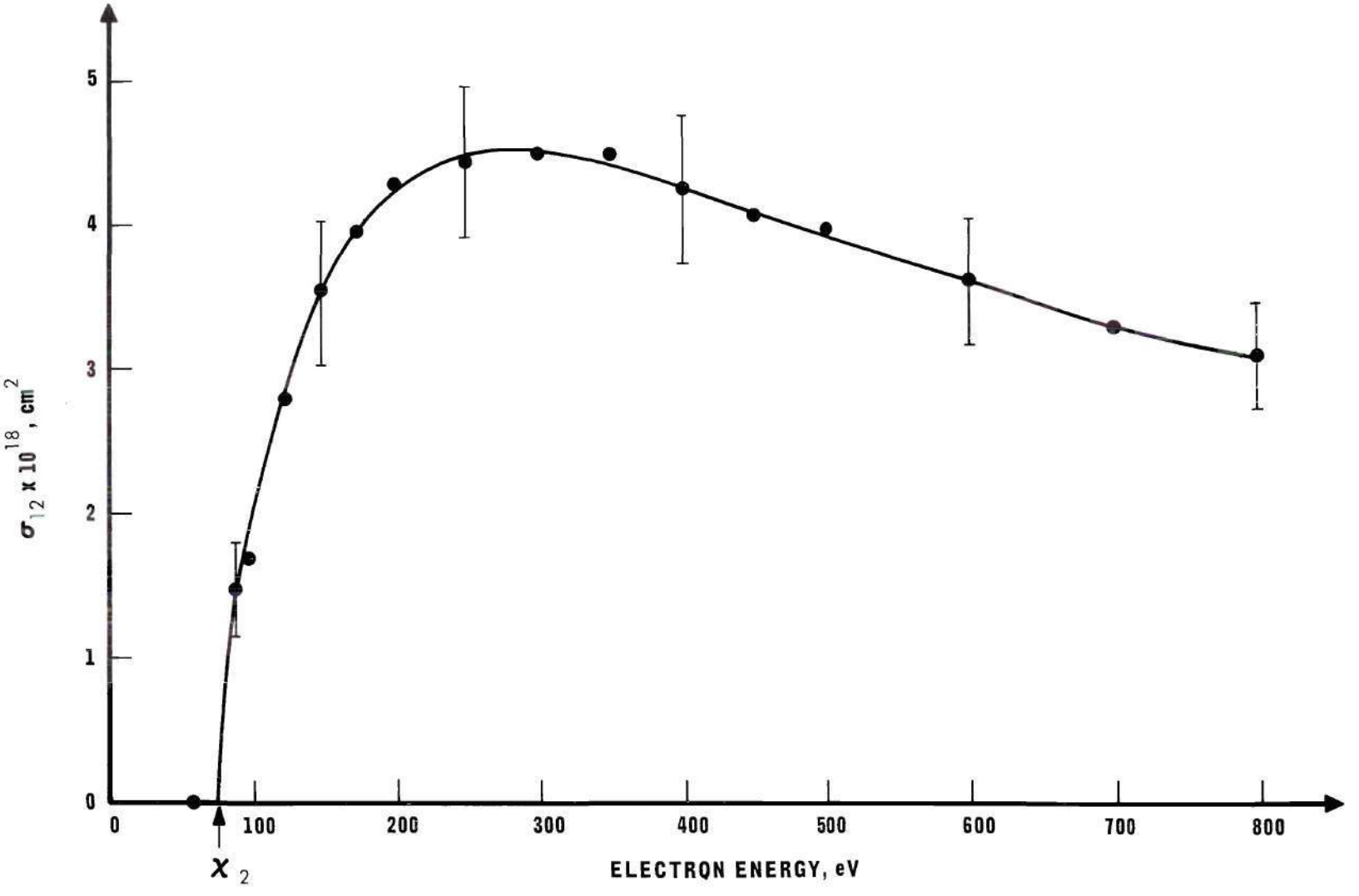

Figure 9. Absolute Cross Sections for the Single Ionization of Li^+ Ions by Electron Impact. The threshold energy for formation of Li^{++} ions is indicated by χ_2.

Indicated Electron Energy, eV	Actual Electron Energy, eV	σ_{12} $\times 10^{18}$, cm^2	Random Error %	Maximum Systematic Error %	Maximum Total Error %
60	57 ±2	0.0	–	–	–
90	87 ±2	1.48	±15	±6	±21
100	97 ±2	1.69	±10	±6	±16
125	122 ±2	2.79	±10	±6	±16
150	147 ±2	3.54	±8	±6	±14
175	172 ±2	3.96	±6	±6	±12
200	197 ±3	4.28	±6	±6	±12
250	247 ±3	4.45	±6	±6	±12
300	297 ±3	4.50	±6	±6	±12
350	347 ±3	4.50	±6	±6	±12
400	397 ±3	4.25	±6	±6	±12
450	447 ±3	4.07	±6	±6	±12
500	497 ±3	3.98	±6	±6	±12
600	597 ±4	3.62	±6	±6	±12
700	697 ±4	3.30	±6	±6	±12
800	797 ±4	3.11	±6	±6	±12

TABLE 1

ABSOLUTE CROSS SECTIONS FOR THE SINGLE IONIZATION OF Li^+ IONS BY ELECTRON IMPACT

of weeks, however, wider variations are seen. These variations can usually be correlated with a deterioration of the degree to which the experimental apparatus satisfies the consistency checks, but it is felt that some weight must still be given to these variations. Accordingly, the random error is increased at 500 eV to $\pm$ 6 per cent. At lower electron energies, where the short term random error is larger, the total random error also is larger, as indicated in Table 1. The total probable error is taken to be the sum of the random and systematic errors. The total probable error in the measurements is estimated to be $\pm$ 12 per cent above 150 eV electron energy; it increases at lower electron energies to $\pm$ 21 per cent at 90 eV. The root mean square error, which is not shown, ranges from $\pm$ 8 per cent at 800 eV to $\pm$ 15 per cent at 90 eV.

In addition to these errors, there also exists some uncertainty in the mean electron energy in the interaction region. Retarding potential measurements show that the electron energy spread is approximately $\pm$ 2 eV about the mean energy. The mean electron energy was determined in the following manner. Both retarding potential measurements and, subsequently, measurements of the electron impact ionization of K^+ ions near threshold were not inconsistent with the assumption that the mean electron energy was about 3 eV less than the indicated energy. Furthermore, the K^+ measurements showed that the magnitude of this energy degradation

must be less than 5 eV. An energy degradation of a few eV is typical of an oxide coated cathode. For these reasons, the mean electron energy in the interaction region is taken to be 3 eV less than the indicated energy; the electron energy has been accordingly corrected in the data presented here. The electron energy is considered to be uncertain by ± 2 eV. This energy uncertainty has not been taken into account in determining the vertical error brackets. While the electron energy uncertainty is insignificant at high energies, at low electron energies it must be considered. The uncertainty in the mean electron energy increases at higher energies, as a consequence of the 0.25 per cent uncertainty in the indicated acceleration voltage.

CHAPTER V

COMPARISONS WITH AVAILABLE THEORY

In this chapter, the present Li^+ results are compared with the existing, relevant theoretical and experimental data. There are presently no other experimental data available on the ionization of Li^+ by electron impact, and so no direct comparison of the experimental results can be made. Moreover, no quantum mechanical calculations for this system are presently available. Thus the comparisons of the Li^+ data must be made either with data for other atomic species or with "universal" electron impact ionization cross section predictions. In either case, such comparisons are most meaningful when made in terms of the "reduced" cross section for the process. The "reduced" cross section is defined as follows.

Let σ_i be the electron impact ionization cross section for a structure having ionization energy I. If ζ is the number of electrons in the shell from which the ionization takes place, then the reduced cross section for this process, $\hat{\sigma}_i$, is defined by

$$\hat{\sigma}_i = \frac{1}{\zeta}\left[\frac{I}{I_H}\right]^2 \sigma_i \qquad (10)$$

where I_H is the ionization energy of atomic hydrogen, 13.60 electron volts. This definition is partially motivated by the investigations of Thomson[31], who employed classical mechanics in his studies of electron impact ionization. The Thomson theory predicts that if

$$u = \frac{E}{I} , \tag{11}$$

where E is the energy of the incident electron, then $\hat{\sigma}(u)$ should be a universal function, valid for any element, whether ionized or neutral. While the functional form predicted by the Thomson theory does not agree with either experimental observations or quantum mechanical predictions, the concept of a "universal" ionization curve appears to have some approximate validity, a fact which has been observed by Elwert[32] and others[33,34]. It is found that if reduced ionization cross sections for a number of elements are plotted as a function of u, then a single curve can be drawn which agrees with all of the experimental data to within about a factor of two. Elwert[32] used these data to deduce an empirical curve which is a good fit over the range $1 \leq u \leq 2$. His formula reads

$$\hat{\sigma}(u) = 2 \frac{u-1}{u^2}\left[1 + 0.3(u-1)\right] \pi a_o^2 \tag{12}$$

where a_o is the radius of the first Bohr orbit of the hydrogen atom. This result is plotted in Figure 10, where it may

be compared with the reduced Li^+ results reported here. The Elwert empirical formula is found to be in very good agreement with the Li^+ measurements over the range in which the Elwert formula is considered valid.

Drawin[33] has also proposed an empirical formula for electron impact ionization cross sections, based upon the concept of the universal ionization curve. The Drawin formula reads

$$\hat{\sigma}(u) = 2.66 f_1 \frac{u-1}{u^2} \ln\left[1.25\ f_2 u\right] \pi a_o^2 \qquad (13)$$

where f_1 and f_2 are two arbitrary constants which may depend on the ionization process under consideration. If no information on the process is known, then f_1 and f_2 should be taken to be unity. The Drawin formula approaches a $\frac{\ln u}{u}$ functional form as u increases; in this respect it is consistent with the Born approximation predictions. Drawin considers his formula to be equally valid over the entire electron energy range. The Drawin empirical formula is plotted with f_1 and f_2 equal to unity in Figure 10. The result is in reasonably good agreement with the Li^+ results throughout the entire energy range. In the near threshold region, however, the Elwert prediction is much better than the Drawin prediction.

For comparison, the Thomson prediction is also shown in Figure 10. The analytic form of the Thomson theory prediction is

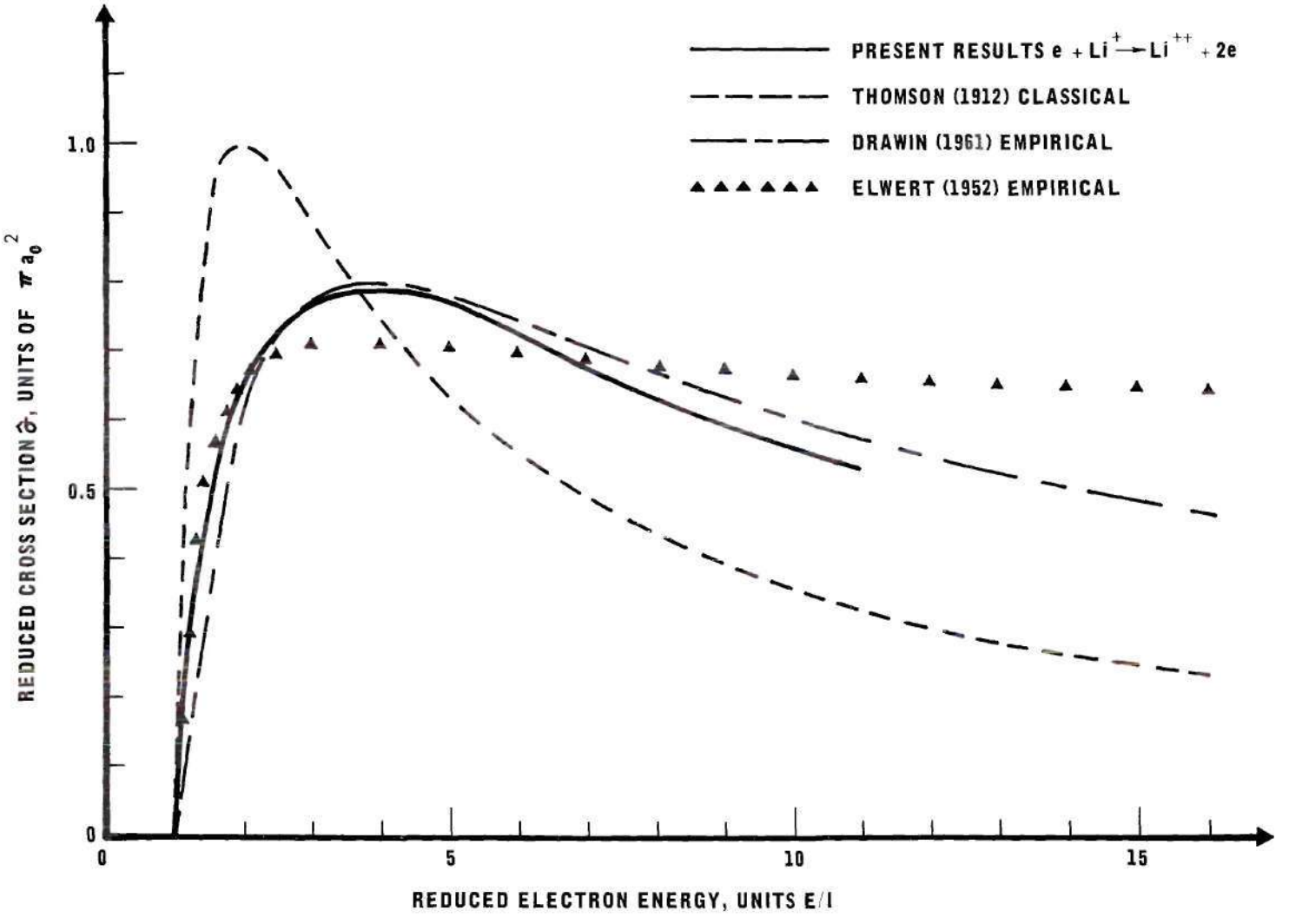

Figure 10. Comparison of the Li^+ Data with Empirical and Classical Predictions.

$$\hat{\sigma}(u) = 4\frac{u-1}{u^2}\,\pi a_o^2 \quad . \tag{14}$$

The Thomson theory is seen to predict too rapid an increase near threshold, and a $\frac{1}{u}$ dependence at high energies, instead of the proper $\frac{\ln u}{u}$ dependence.

Burgess and Rudge[7,8] have calculated the cross sections for the ionization of hydrogenic positive ions by electron impact in the Coulomb-Born-Oppenheimer approximation. They find that the reduced cross sections, $\hat{\sigma}(u)$, for all the hydrogenic ions approach the same analytic form, in the limit of large electron impact energy. In this limit the effects of the different nuclear coulomb fields of the several hydrogenic ions become insignificant. The scaling relation suggested by the Thomson theory appears to be valid for hydrogenic positive ions in the limit of large electron energies. The He^+ calculations of Burgess and Rudge[7,8] approach the experimental He^+ results of Dolder, Harrison and Thonemann[4] at the highest electron energies attained, while overestimating the cross sections at lower energies, in the manner typical of Born approximation calculations.

The Dolder, Harrison, and Thonemann reduced He^+ cross sections agree closely at high electron energies with the reduced H atom electron impact ionization cross sections measured by Fite and Brackmann[3]. The hydrogen atom and the helium ion are, of course, adjacent members of the hydrogen-like isoelectronic sequence. It is of interest to compare

the reduced cross sections for electron impact ionization of Li^+ and of He, which are also isoelectronic to one another. This comparison is made in Figure 11, where use is made of the experimental results of Smith[35] for He. At the highest electron energy attained in the Li^+ measurements, the reduced He and Li^+ cross sections coincide. At lower electron energies the Li^+ cross sections are substantially higher than the He cross sections. The increase is presumably due to the focusing action of the ionic field of the lithium ion, as can be seen from the following simple model. The long range Li^+ ionic field tends to attract slow electrons toward the ion, thus increasing the probability of ionization above that expected in the absence of such a field. At high electron energies, however, the electrons undergo very small deflections in this field, and the net effect of the ionic field is small.

In Figure 11, the Li^+ measurements are also compared with the He^+ measurements of Dolder, et al.[4] The reduced He^+ cross sections are seen to increase more rapidly and to have a sharper peak at a lower reduced electron energy than the reduced Li^+ cross sections. The high electron energy behavior of both curves is similar, however.

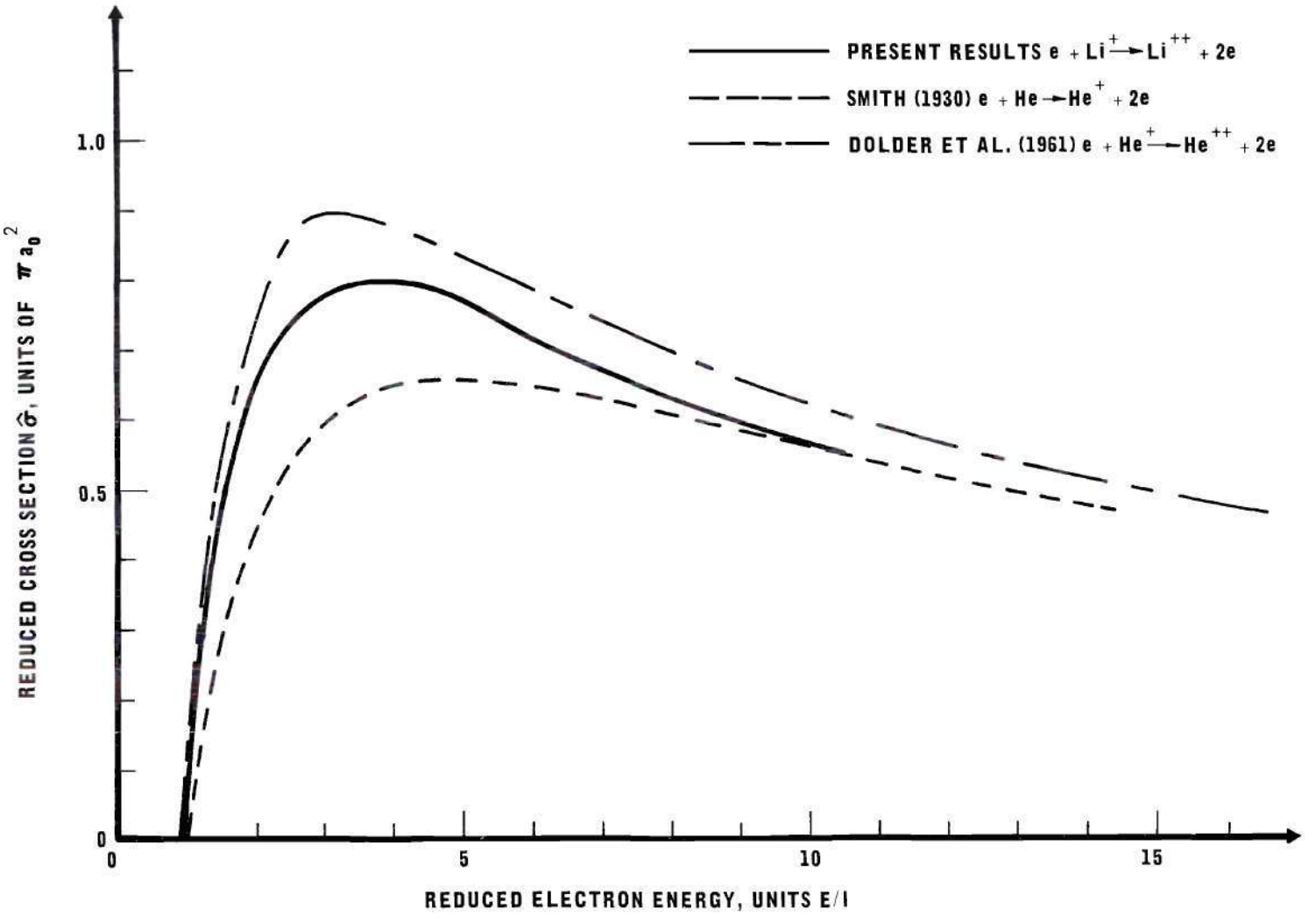

Figure 11. Comparison of the Li^+ Data with Experimental He and He^+ Results.

CHAPTER VI

CONCLUSIONS

The absolute cross sections for the ionization of Li^+ ions by electron impact have been measured for electron energies over the range from near threshold to 800 eV. These measurements were performed under continuous beam conditions in a crossed beam facility operating at a residual gas pressure of about 10^{-8} Torr. This research represents the first successful absolute cross section measurements both involving crossed charged particle-charged particle beams and performed under continuous beam conditions.

The experimental results are presented graphically in Figure 9 and in tabular form in Table 1. The maximum error in the measurements is estimated to be $\pm$ 12 per cent above 150 eV electron energy, the possible error increasing to $\pm$ 21 per cent at 90 eV. Of this total possible error, an amount $\pm$ 6 per cent is considered systematic. Checks were performed to evaluate the possible effects of such parameters as the continuous beam measurement technique, beam intensities, beam profiles, space charge, signal-to-noise ratio, and ion beam composition.

The Li^+ results are compared with the classically scaled experimental ionization cross sections for He and He^+

in Figure 11. Atomic helium and singly ionized lithium are, of course, two adjacent members of the isoelectronic helium-like sequence. The classically scaled Li^+ and He cross sections coincide at our highest electron energy, where the effect of the Li^+ coulomb field is becoming negligible. The same sort of agreement was found by Dolder, Harrison, and Thonemann,[4] when they compared their He^+ results to the scaled isoelectronic H atom ionization measurements of Fite and Brackmann[3].

The Li^+ results are compared with the empirical predictions of Drawin[33] and Elwert[32] in Figure 10. The Drawin prediction is in fair agreement with the Li^+ data throughout our energy range. The Elwert empirical formula is not expected to be in good agreement above two times the threshold energy. Below two times threshold, however, the Elwert formula is in excellent agreement with the Li^+ data.

APPENDIX I

DERIVATION OF σ_{12} IN TERMS OF EXPERIMENTAL PARAMETERS

In this section an expression for the cross section for single ionization of ions by electron impact will be developed in terms of experimentally observed parameters. With obvious modifications this expression can be utilized for any crossed beam experiment. Before the development can proceed it is necessary to define a collision cross section. This definition will be obtained by a technique differing only slightly from that employed by McDaniel[36].

Consider a parallel beam of monoenergetic projectiles approaching the origin of the laboratory coordinate system, as shown in Figure 12. The beam is traveling parallel to the x-y plane, but is inclined at an angle Θ to the y-axis. The beam is uniformly composed of particles of number density n particles/cm^3 and speed V cm/sec in the laboratory frame of reference. Let N_p be the total number of these projectiles which pass through a 1 cm^2 area in the x-z plane per second. The particle flux and the number density are related by the equation

$$N_p = nV \cos \Theta \qquad (15)$$

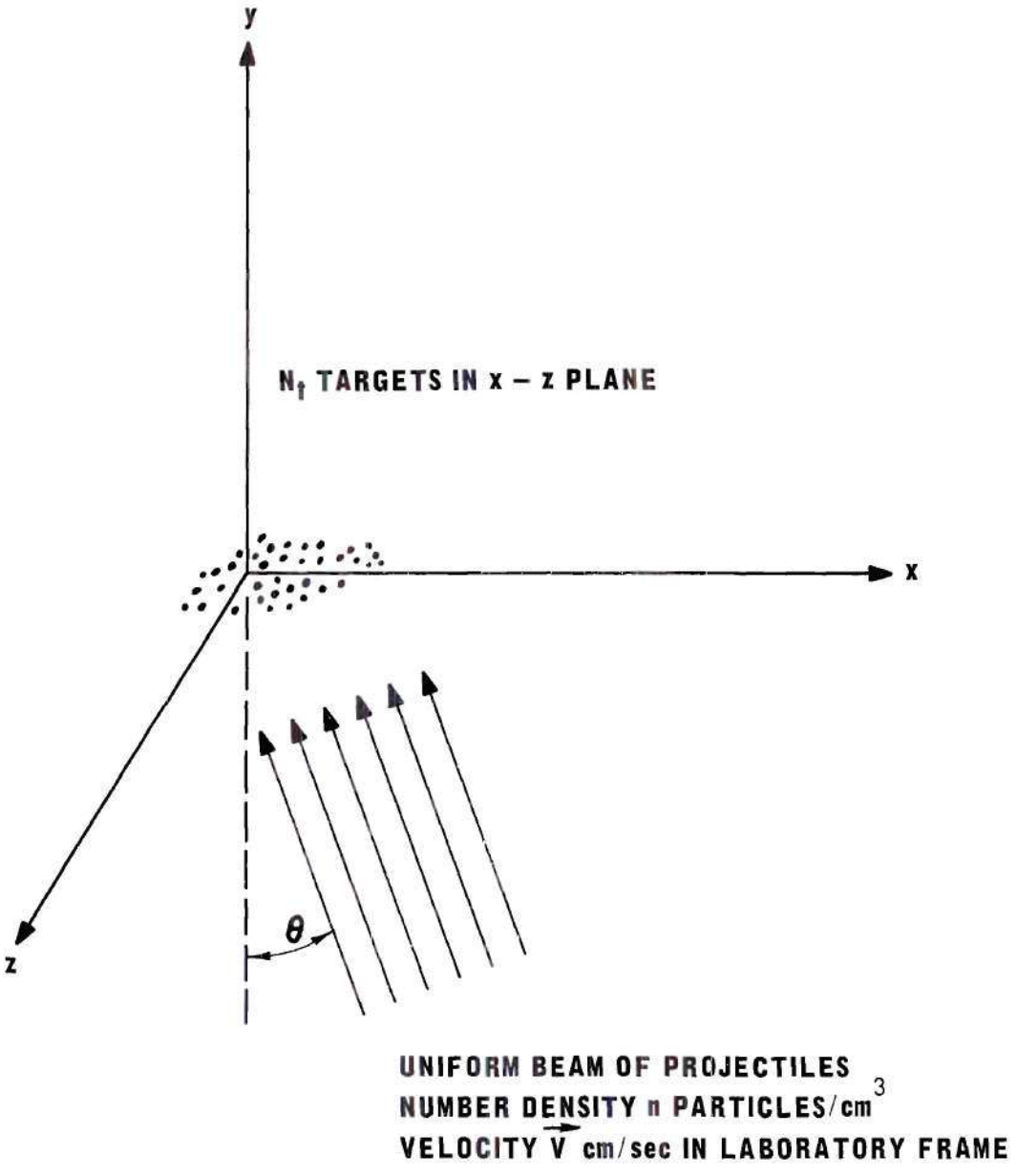

Figure 12. The Laboratory Coordinate System in which the Ionization Cross Section will be Defined.

Consider N_t targets to be located in that region of the x-z plane through which the projectile beam passes. We assume that there are sufficiently few targets present to ensure that none is shielded by another and that no projectile interacts with more than one target. We further assume that the interactions do not remove any of the targets, so that N_t will remain constant. The cross section for a particular projectile-target interaction "r" can now be defined. It is apparent that the number of interactions r occurring per second, R, is directly proportional to both N_p and N_t. Inserting a constant of proportionality σ, we may write

$$R = \sigma N_p N_t \tag{16}$$

This expression is the defining relation for σ, the cross section for interaction r. The cross section has the dimensions cm^2, from whence arises its name. It is a measure of the probability of the interaction r taking place.

With the aid of this definition, an expression for the cross section for the single ionization of ions by electron impact can now be developed. Consider a rectangular xyz coordinate system in the laboratory frame of reference. Let a monoenergetic uniform beam of ions traveling in the +y direction be intersected normally by a monoenergetic uniform beam of electrons traveling in the +x direction. The ion and electron velocities are $\vec{V}_i$ and $\vec{V}_e$ cm/sec, respectively, in the laboratory frame of reference. The physical

extent of the ion beam is over $o \leq z \leq h$ and $o \leq x \leq w$, while that of the electron beam is over $o \leq z \leq h$ and $o \leq y \leq \ell$. If the total electron current is J amperes, then the number density in the electron beam is given by

$$n_e = \frac{J}{\ell h e V_e} \frac{\text{electrons}}{\text{cm}^3} \tag{17}$$

where e is the magnitude of the electronic charge. In order to phrase this problem in such a form that Equation (16) is applicable, it will be necessary to transform the problem to a frame of reference in which one of the particle beams is stationary. Since $V_e >> V_i$ in general, we shall transform to a frame in which the ion beam is stationary. This new frame will be referred to as the ionic rest frame.

Following this transformation, the collision region appears, at a given instant of time, as shown in Figure 13. In this frame the electron beam is traveling upward and to the left with velocity $\vec{V}'$ cm/sec; consequently any reacted targets are effectively replenished, while the total number of ions in the path of the electron beam, N_t, remains constant. Since multiple interactions do not occur as a result of the tenuous nature of the ion beam, the ion beam width w is neglected and the ions are shown in a linear array. The geometry of this transformed system is one in which Equation (16) is directly applicable. We can proceed to determine the quantities appearing in this expression, and

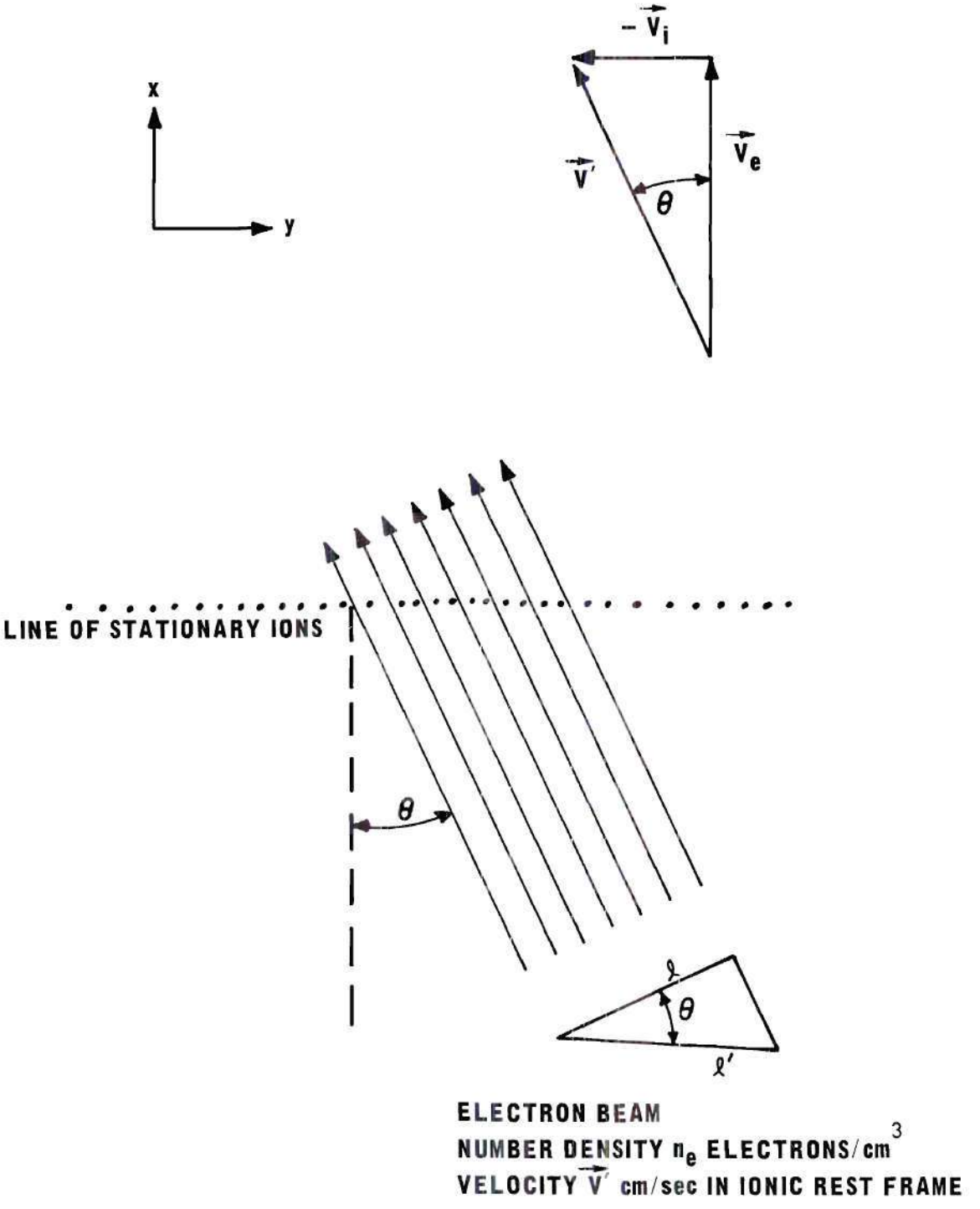

Figure 13. View of the Collision Region in the Ionic Rest Frame at a Given Instant of Time. The ion and electron velocities in the laboratory frame are $\vec{V}_i$ and $\vec{V}_e$, respectively.

then solve for the desired cross section.

In the ionic rest frame, the electrons have a velocity $\vec{V}'$ cm/sec, whose magnitude is given by the equation

$$V' = (V_e^2 + V_i^2)^{\frac{1}{2}} \text{ cm/sec.} \tag{18}$$

The electron number density n_e, however, remains invariant under the transformation to the ionic rest frame. The number of electrons per second crossing unit area in the plane of the ions is seen to be

$$N_p = \frac{n_e V' \ell}{\ell'} \tag{19}$$

$$= \frac{J}{eh\ell'} \frac{V'}{V_e} \tag{20}$$

where use has been made of Equation (17) in obtaining Equation (20). As is evident from Figure 13, the length ℓ' is the projection of ℓ on the stationary line of ions.

The total number of ions N_t present in that portion of the ion beam through which the electron beam is passing at any given instant is given by

$$N_t = \frac{I^+}{e} \frac{\ell'}{V_i} \text{ ions,} \tag{21}$$

where I^+ is the total ion current. The interaction of interest here is the single ionization of the ions; the

total number of reactions per second is given by

$$R = \frac{I^{++}}{2e} \quad \text{ionizing collisons/sec} \tag{22}$$

where I^{++} is the total current of doubly-ionized particles produced by electron impact. The factor of 2 arises as a result of the double charge on these ions. Equations (20), (21) and (22) may now be substituted directly into Equation (16); following this substitution, and some simplification, we obtain

$$\frac{I^{++}}{h} = 2\sigma_{12} \frac{V'}{eV_i V_e} \frac{I^{+}}{h} \frac{J}{h} . \tag{23}$$

It is noted that each of the beam currents appearing in this equation is divided by the height of that beam; each of these quotients thus has dimensions of a linear current density. Equation (23), however, applies only to the highly idealized case of uniform beams of the same height. If we now consider ion and electron beams whose linear current densities are functions of z, then, to a first approximation, Equation (23) is valid for any small segment, say z to z + h, of the non-uniform beams. If h is allowed to approach zero, the quotients in Equation (23) become linear current densities, and Equation (23) can be rewritten as

$$i^{++}(z) = 2\sigma_{12} \frac{V'}{eV_i V_e} i^{+}(z) j(z) , \tag{24}$$

valid for all z, and for beams whose current densities are nonuniform in z. The lower case "i" and "j" represent linear current densities. Integrating Equation (24) and noting that the coefficient of $i^{+}(z)j(z)$ is not a function of z, we obtain

$$\int_{-\infty}^{\infty} i^{++}(z)dz = 2\sigma_{12} \frac{V'}{eV_e V_i} \int_{-\infty}^{\infty} i^{+}(z)j(z)dz. \qquad (25)$$

The left hand side of Equation (24), however, is the total doubly-ionized signal current, I^{++}. Using this result, together with Equation (18), and solving for σ_{12}, we finally obtain

$$\sigma_{12} = \frac{eV_i V_e}{2\left[V_i^2 + V_e^2\right]^{\frac{1}{2}}} \frac{I^{++}}{\int_{-\infty}^{\infty} i^{+}(z)j(z)dz} \qquad (26)$$

which is the desired result.

As was discussed in Chapter II, it is more convenient to write Equation (26) in the form

$$\sigma_{12} = \frac{eV_i V_e}{2\left[V_i^2 + V_e^2\right]^{\frac{1}{2}}} \frac{I^{++}}{I^{+}J} F \qquad (27)$$

where

$$F = \frac{\int_{-\infty}^{\infty} i^{+}(z)dz \int_{-\infty}^{\infty} j(z)dz}{\int_{-\infty}^{\infty} i^{+}(z)j(z)dz} . \qquad (28)$$

All quantities except the form factor F are directly observable experimental parameters. The form factor F is approximated with the aid of a beam scanner, as shown in Figure 1. The remainder of this appendix will be devoted to obtaining a suitable approximation.

It should first be noted that the integrands in Equation (28) will in reality always be zero outside some finite interval. Thus no problems involved with approximating improper integrals arise here; the infinite limits may be ignored. Let the range of integration in Equation (28) be uniformly partitioned into segments of length Δz. Then F may be approximated by

$$F \cong \frac{\Delta z \sum_k i_k^{+} \sum_k j_k}{\sum_k i_k^{+} j_k} \qquad (29)$$

where i_k^{+} is the average ion current density in the k^{th} partition and j_k is the average electron current density in the k^{th} partition.

If a movable slit scanner, with ion slit height h_i and electron slit height h_e, were positioned such that the

slits were centered on the k^{th} partition, then

$$i_k^+ \cong \frac{I_k^+}{h_i} \tag{30}$$

and

$$j_k \cong \frac{J_k}{h_e} \ . \tag{31}$$

where I_k^+ is the positive ion current passing through the ion slit in the k^{th} position and J_k is the electron current passing through the electron slit in the k^{th} position. Upon substitution of these expressions in Equation (29), the slit heights cancel and there results

$$F \cong \frac{\Delta z \sum_k I_k^+ \sum_k J_k}{\sum_k J_k I_k^+} \tag{32}$$

Thus if the slit scanner is moved across the beams in uniform steps of length Δz, the resulting ion and electron currents, measured as a function of slit position, can be used in Equation (32) to calculate F. This last expression is the desired approximation to F. It is important to note that the only relevant dimension in this expression is the spacing between slit positions, Δz; other

dimensions, such as the overall height of the ion beam and the heights of the scanning slits, cancel out.

APPENDIX II

TYPICAL MEASUREMENT DATA

The data taken during a typical run are presented in Tables 2 and 3. The purpose of these data is to show typical operating conditions and data scatter during one run.

A few remarks must first be made in order to clarify some of the items in Table 2. The "Ion Beam Convergence" is the percentage increase in the measured Li^+ current as the electron current is increased from zero to the indicated quantity. An electron beam current of 10 ma. is more than adequate to eliminate all ion beam losses. Thus the percentage increase observed in the ion beam intensity when the electron beam intensity is increased from zero to 10 ma. indicates the total particle loss from the ion beam when no electrons are present.

The "Slow Electron Correction" arises in the following manner. Whenever the electron beam is operating, the vacuum chamber is filled with a gas of "cold" electrons; some of these electrons strike the unshielded electron Faraday cup, producing an electron current which is not a part of the energetic primary electron beam. The fractional magnitude of this current relative to the total electron current is determined by applying a potential to make the electron Faraday cup a few volts negative with respect

DATA SHEET NUMBER 57–36 Date 1/2/65

RUN b Time 8 PM

Electron Energy 250 eV

Electron Current, J, 1.96×10^{-3} A

Screen Grid 0 V w.r.t. Ground

Slow Electron Correction (S.E.C.) 1.04

Electron Cup Aperture Current < .01 ma

Ion Emitter Temperature 1000°C

Li^{++} Aperture Voltage –67 V

Electrostatic Analyzer Voltage 700 V

Ion Energy 1000 eV

Ion Current 2.00×10^{-7} A

Ion Extraction Voltage 22 V

Horizontal Deflectors ±45.5 V

Vertical Deflectors ±8.5 V

Vertical Focus Voltage –25 V

Ion Beam Convergence with 2 ma. Electron Beam < 1/2%

Ion Beam Convergence with 10 ma. Electron Beam < 1%

I^{++} BEAM CURRENT MEASUREMENTS

Measurement No.	1	2	3	4	5	6	7	8
	I^{++} (I, 0)	I^{++} (I, e)	I^{++} (I, 0)	I^{++} (I, e)	I^{++} (I, 0)	I^{++} (I, e)	I^{++} (I, 0)	I^{++} (I, e)
	1.41×10^{-15} A	2.17×10^{-15} A	1.46	2.19	1.47	2.22	1.44	2.21
I^{++}_{sig} (I, 3)	2.25×10^{-15} A	2.20	2.22	2.21	2.24	2.27	2.26	

Average I^{++}_{sig} (I, e) = $2.24 \pm .04 \times 10^{-15}$ A

Total Random I^{++}_{sig} (I, e) Error = $\pm .08 \times 10^{-15}$ A

Average I^{++} (0, 0) = $-0.65 \pm .01 \times 10^{-15}$ A

Average I^{++} (0, e) = $-2.14 \pm .04 \times 10^{-15}$ A

I^{++} Net Electron Current $-1.49 \pm .04 \times 10^{-15}$ A

$$\sigma_{12} = 2.66 \times 10^{-12} \times \frac{I^{++}_{sig} \times F \times (S.E.C.)}{2 \times I^{+} \times J} = \frac{2.66 \times 10^{-12} \times 2.24 \pm .08 \times 10^{-15} \times .565 \times 1.04}{2 \times 2 \times 10^{-7} \times 1.96 \times 10^{-3}} = 4.47 \pm .08 \times 10^{-18} \text{ cm}^2$$

TABLE 2

TYPICAL CROSS SECTION MEASUREMENT DATA

SCANNER DATA SHEET

REFERS TO DATA SHEET 57-36

TAKEN IMMEDIATELY (BEFORE) (AFTER) RUN NO. b

Micrometer Position, inches	I_K^+, A	J_K, A	$I_K^+ J_K$, A^2
.740	0×10^{-9}	$.000 \times 10^{-3}$	$.000 \times 10^{-12}$
.760	.45	.000	.000
.780	2.8	.000	.000
.800	8.25	.003	.025
.820	16.0	.045	.720
.840	17.9	.134	2.399
.860	18.5	.201	3.718
.880	19.0	.277	5.263
.900	19.5	.307	5.986
.920	19.25	.311	5.987
.940	18.1	.281	5.086
.960	16.0	.259	4.144
.980	13.2	.183	2.416
1.000	10.4	.026	.270
1.020	7.6	.000	.000
1.040	5.7	.000	.000
1.060	3.8	.000	.000
1.080	1.2	.000	.000
1.100	0.0	.000	.000
ΔM, inches	$\sum_K I_K^+$, A	$\sum_K J_K^+$, A	$\sum_K I_K^+ J_K^+$, A^2
.020	197.7×10^{-9}	2.027×10^{-3}	36.014×10^{-12}

	Before Scan	After Scan
I^+	2.00×10^{-7} A	1.98×10^{-7} A
J	2.00×10^{-3} A	2.04×10^{-3} A

$$F = \frac{\int_{-\infty}^{\infty} i^+(z)dz \int_{-\infty}^{\infty} j(z)dz}{\int_{-\infty}^{\infty} i^+(z)j(z)dz} \cong \frac{2.54\,\Delta M \sum_K I_K^+ \sum_K J_K}{\sum_K I_K^+ J_K} = 0.565$$

TABLE 3

TYPICAL BEAM PROFILES

to ground. The "Slow Electron Correction" to the measured cross section is then $\frac{1}{1-x}$, where x is the fractional decrease in the collected electron current observed upon application of the retarding potential. The "Slow Electron Correction" enters as a multiplicative factor into the cross section calculation.

All currents to the Li^{++} detector are measured by use of the rate-of-charge mode; only the results of the current calculations are shown, since a typical recorder trace has already been exhibited in Figure 7. The quantities $I^{++}(I,0)$ and $I^{++}(I,e)$ are measured sequentially, and a total of four measurements are made for each current, as seen in the table. The quantity $I^{++}_{sig}(I,e)$ is determined from

$$I^{++}_{sig}(I,e) = I^{++}(I,e) - I^{++}(I,0) - \left[I^{++}(0,e) - I^{++}(0,0)\right]_{ave}$$

as was deduced in Chapter IV. The expression in brackets is the average net electron current to the Li^{++} cup. Each of the currents in the brackets is measured three times, and an average value for the indicated difference is determined. This average net electron current to the Li^{++} cup is used, together with an adjacent pair of $I^{++}(I,e)$ and $I^{++}(I,0)$ currents, to calculate a value for $I^{++}_{sig}(I,e)$. Seven such determinations of this signal current are possible. The average value of these seven determinations of

$I^{++}_{sig}(I,e)$ is then used to compute the ionization cross section. This calculation also requires knowledge of the form factor F, data for which are presented in Table 3. Since in this case the heights of the scanning slits are the same as the spacing between micrometer positions, the sums of the ion and electron currents observed at the several micrometer positions should equal the total ion and electron currents, respectively. This fact is used as a partial check on the accuracy of the scanner data.

The cross section calculations appear near the bottom of Table 2. The scatter in the results in this case indicates a short term random measurement uncertainty of approximately $\pm$ 2 per cent.

APPENDIX III

OPERATIONAL PROCEDURES FOR OXIDE CATHODES IN DEMOUNTABLE VACUUM SYSTEMS

Several excellent sources of information on electron tube technology are available; among these special attention is called to the book by Kohl[37] and the MIT Tube Laboratory Manual.[38] The material which follows is taken partly from these sources and partly from experience gained in the course of this experiment. It is hoped that this discussion will be of some value to workers unfamiliar with the use of oxide cathodes in demountable vacuum systems.

The oxide cathode is an n-type semiconductor consisting of a mixture of barium, calcium and strontium oxides on a nickel base. The presence of free barium in the structure is an essential requirement for the low work function characteristic of oxide cathodes.

The mechanisms active in producing this free barium are extremely sensitive to hydrocarbon contamination at normal operating temperatures (~850 ^{o}C). Such contamination is generally irreversible, and must be carefully avoided. Hydrocarbon contamination is not necessarily fatal at lower temperatures, as slow heating may drive the hydrocarbons off the cathode before the threshold temperature for the

irreversible reactions is reached.

In addition to this type of poisoning, we also find that the alkaline oxides of the cathode are unstable on exposure to air. The oxides pick up a water molecule, forming the hydroxide; the hydroxides (except for Ca) in turn pick up H_2O to form the hydrate.[39] The reversal of this process is that of cathode activation, a subject which will be discussed shortly.

Haas and Jensen[39,40] have investigated the repeated activation and deactivation of oxide cathodes. They find that a major cause of failure to reactivate satisfactorily is flaking of the oxide coating. They further identify the primary cause of this flaking action to be lattice distortion resulting from taking up waters of hydration. It is found that, provided the cathode temperature is held above 150 °C during exposure to air, the formation of the hydrates is prevented, and the number of possible successful reactivations is greatly increased.

In our apparatus this precaution is followed, and the 6L6 cathode is kept at approximately 150 °C at all times during exposure to air. A heater voltage of 1.3 volts ac serves nicely in this case. During the 24-hour chamber bakeout this heater voltage is not changed. After 24 hours the zeolite trap bakeout is stopped and the trap is allowed to cool for approximately 2 hours. At this point, the cathode temperature is slowly increased, over a period of about one

hour, to 750 ^{o}C, the pressure being kept below 1 x 10^{-6} Torr. By this time, the onset of conversion of the hydroxides to the oxides may be seen. The conversion takes place primarily over the temperature range 750 ^{o}C - 900 ^{o}C, and entails large pressure increases. The cathode temperature is slowly increased to 900 ^{o}C, while the pressure is kept below 5 x 10^{-5} Torr; one should wait for the pressure to stabilize at each temperature level before proceeding. Following conversion of the hydroxides, the pressure falls rapidly, by perhaps two orders of magnitude in a few minutes. This precipitous drop is indicative of a well converted cathode. At this point the vacuum chamber bakeout is stopped. After the pressure has reached the mid 10^{-7} Torr range, cathode activation proceeds. The cathode is flashed to 1100 ^{o}C for a period of one minute, and then reduced to 900 ^{o}C for a one minute period. This process is repeated several times; its purposes are to ensure that the hydroxide conversion is complete and to produce free barium at the metal-semiconductor interface. The free barium then diffuses throughout the semiconductor, as is required to obtain low work function electron emission. The cathode temperature is now reduced to its normal 850 ^{o}C operating temperature.

A 500 V accelerating potential is applied and an electron current is drawn while keeping the indicated pressure below 1 x 10^{-6} Torr. The latter precaution is necessary to prevent ion bombardment damage of the cathode. The electron

current is increased to 10 milliamperes as rapidly as the pressure constraint will allow. In order to outgas surfaces which the electron beam strikes, the source is left in operation at 10 ma. while the chamber cools. This technique has proved very successful in producing an electron source which does not greatly perturb the chamber pressure when turned on and off. One word of caution should be added, however. The oxide cathode should not be allowed to remain at its operating temperature during a second bakeout of the zeolite trap. If the temperature is not reduced before baking the trap, the released hydrocarbons will generally permanently poison the cathode. Such a poisoned cathode is easily recognized by its dark gray color.

APPENDIX IV

BEAM PULSING SCHEMES

Whereas this experiment utilized continuous ion and electron beams, there exist several beam pulsing schemes which might have been employed in the measurements. It is of interest therefore to consider these various pulsing schemes, and to compare them to the continuous beam technique. Such a comparison will be made in the remainder of this appendix.

The primary detrimental effects occurring in the beam intersection region are the space charge interactions of the beams, and the background pressure changes resulting from turning one beam off and on. It is to these effects that the measurement techniques must address themselves. In order to facilitate this comparison, measurements of the following hypothetical event will be compared using the various measurement schemes. This event is the single ionization of ions by electron impact at a particular ion and electron energy. Continuous ion and electron currents of 1.0×10^{-7}A and 1.0×10^{-3}A respectively are assumed to produce 0.5×10^{-15}A of doubly-ionized ions as a result of electron impact ionization. The 1.0×10^{-7}A ion beam produces a noise current at the doubly-ionized particle detector of 1.0×10^{-15}A; this

current is composed both of doubly-ionized ions which have been produced by charge stripping on the background gas, and of stray singly-ionized ions which have reached the doubly-ionized particle detector. The continuous beam measurement will be considered first, followed by the pulsed beam measurements.

Continuous Beams

Since continuous beam measurements have been discussed in detail in Chapter IV, only the pertinent conclusions will be presented here. The continuous beam measurement assumes that the ionization signal current is given by the difference between I^{++} with ion and electron beams on and I^{++} with only the ion beam on. Since the presence of the electron beam increases the chamber pressure, the charge-stripped portion of the I^{++} noise current is larger when the electron beam is on than it is when the electron beam is off. The measured ionization signal current is thus too large by the amount of this increase. In order for this error to be small, it is generally necessary that the experiment be performed in an ultra-high vacuum environment. This pressure dependent error is shown to be not serious if continuous beam measurements at electron energies below the ionization threshold energy yield apparent cross sections which are insignificant compared with those obtained well above threshold. In addition to this pressure dependent error, the deflection of ions by the space

charge of the electron beam may cause the noise current to the doubly-ionized particle detector to change in the presence of the electron beam. Thus electron beam space charge effects can also produce a measurement error. Measurements below threshold can again be utilized to determine whether the magnitude of such an error is significant.

If such errors were not present, then the continuous beam measurement should yield the correct ionization signal current. The ionization signal to ion beam noise measurement ratio (SNR) would be given by

$$SNR = \frac{I^{++}(I,e) - I^{++}(I,0)}{I^{++}(I,0)} \tag{33}$$

$$= \frac{1.5 \times 10^{-5} - 1.0 \times 10^{-15}}{1.0 \times 10^{-15}} = 0.5.$$

Pulsed Beams

It can be easily shown[41] that a vacuum chamber of volume V liters, being pumped at S liters per second, has a time constant τ for pressure changes given by

$$\tau = \frac{V}{S} \text{ seconds.} \tag{34}$$

If a particle beam in this chamber is pulsed on and off with a period much less than τ, the the system pressure does not change appreciably from an "on" cycle to an "off" cycle, but rather the system assumes an average pressure.

The one advantage of all beam pulsing schemes over the continuous beam measurements lies in the fact that it is possible to allow the vacuum system to attain an average steady pressure. Thus an increase in charge-stripped currents resulting from pressure changes need not be a source of error.

Typical pulsing rates are on the order of a few kilocycles per second. At this rate the length of one pulse of beam particles is typically far greater than the size of the experimental apparatus. Thus the pulsed beam in the apparatus must not be thought of as a series of short beam segments; rather, a continuous beam of particles is either filling the apparatus, or it is not. Schematic diagrams of beam pulsing schemes generally show a number of pulses in the diagram, but it must be remembered that such a diagram is on a scale far larger than that of the experimental apparatus. As a consequence of these beam pulse lengths, the effects of the electron space charge mentioned in connection with continuous beam measurements are still present in all beam pulsing schemes. Thus whenever pressure changes do not present a significant source of error, the continuous beam measurement technique is equal to or better than any pulsed beam measurement technique.

The possible beam pulsing schemes include pulsed ion beams, pulsed electron beams, and pulsed ion and electron beams. These cases will be considered separately and compared to the continuous beam measurements by means of the

hypothetical experiment described previously. The question naturally arises as to how the intensities of the pulsed and continuous beams should be related, in order to obtain the most meaningful comparisons between pulsed and continuous beam measurements. The comparisons could be based on either the peak currents or the mean currents being equal in the measurement schemes being compared. Since the magnitude of the electron beam space charge convergence effect is determined by the magnitude of the electron current during the time at which both beams are present in the interaction region, the comparisons in all cases are based on this peak electron current, rather than the mean current, being equal.

Pulsed Electron Beam

A schematic diagram depicting the various particle currents in the case of a pulsed electron beam is presented in Figure 14a. It is noted that the desired ionization signal, shown in crosshatch, is present as a time varying component on a steady background. Sufficient information is present to extract this component, provided that either the I^{++} current can be measured as a function of time, or phase-sensitive detection techniques can be applied. Unfortunately the 10^{-15} ampere level of this signal is smaller than the present technological capabilities of phase-sensitive detectors. It would, however, be possible to measure the I^{++} signal current using a multiplier as a particle counter and appropriately gating the particle pulses to two scalers. The difference in the count rate of the two scalers would then represent the desired

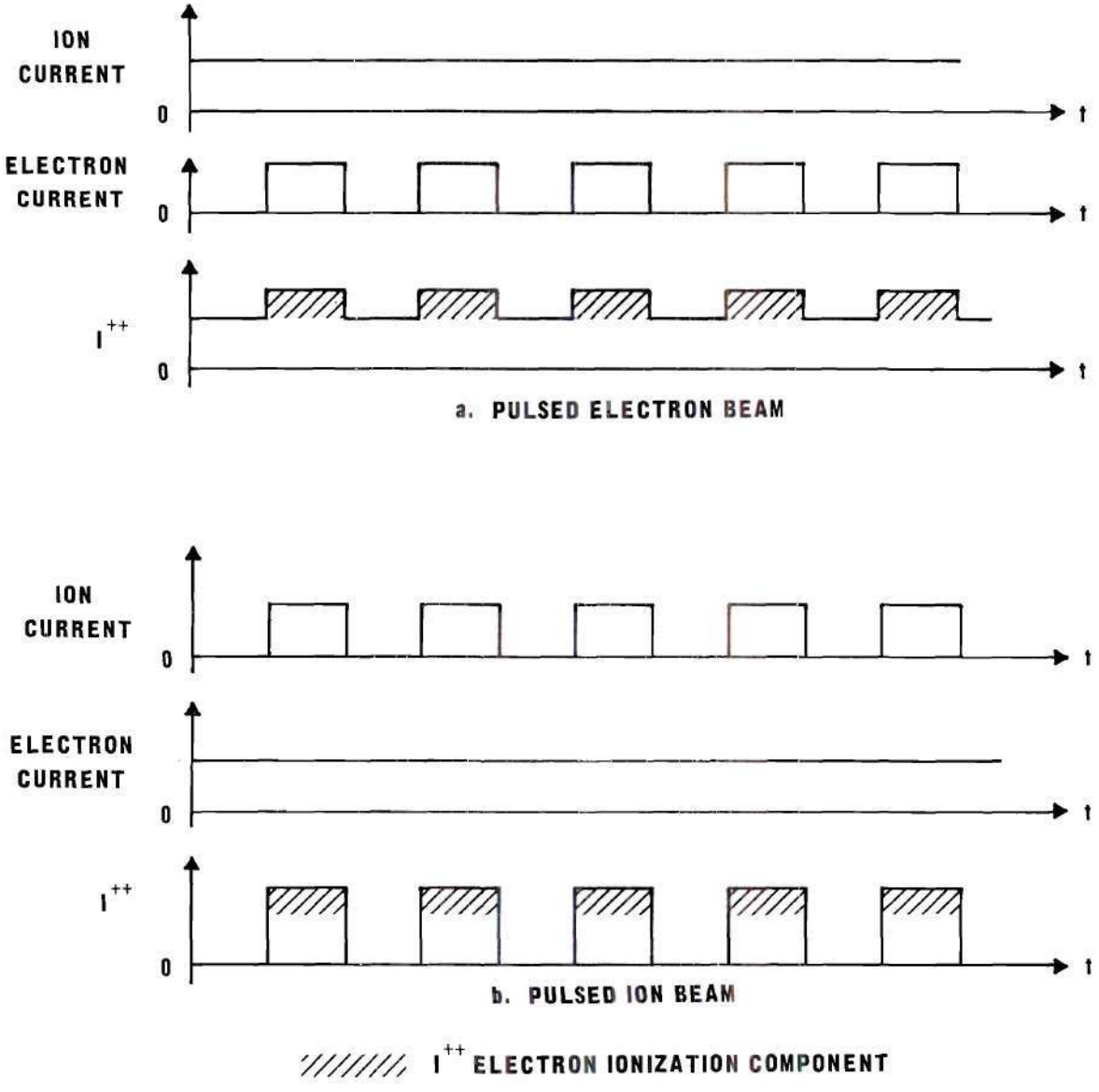

Figure 14. Current Waveforms Applicable to Pulsed Electron Beam Experiments and to Pulsed Ion Beam Experiments.

signal. The use of a multiplier, however, introduces the additional uncertainty of the efficiency of the multiplier. The converging effects of the electron beam space charge, if significant, will give rise to a non-electron-impact ionization current which is in phase with the electron beam pulses. Thus, if such space charge effects are present, they will give rise to a measurement error, such as occurred in the case of the continuous beam measurements.

Pulsed Ion Beam

The appropriate waveforms for the case of a pulsed ion beam are shown in Figure 14b. It is apparent that there is insufficient information present to separate the electron impact ionization current from the ion beam noise current. Thus this case need be considered no further.

Pulsed Ion and Electron Beams

The crossed beam experiments of Dolder, Harrison, and Thonemann[4,5,6] utilized pulsed ion and electron beams, in the manner shown in Figure 15a. The ion beam was pulsed at 5 kc, with a 50 per cent duty cycle, while the electron beam was pulsed at the same frequency, but with a 25 per cent duty cycle.* The pulsing frequency is sufficiently high to ensure a steady pressure in the vacuum chamber. The phase of the electron beam is adjustable with respect to that of the

*The duty cycle for one of the beams should be less than 50 per cent in order to avoid beam synchronization difficulties. However these difficulties could still be easily avoided with a duty cycle of 40 per cent, and, as will be evident, the signal to noise ratio would be improved over the 25 per cent case.

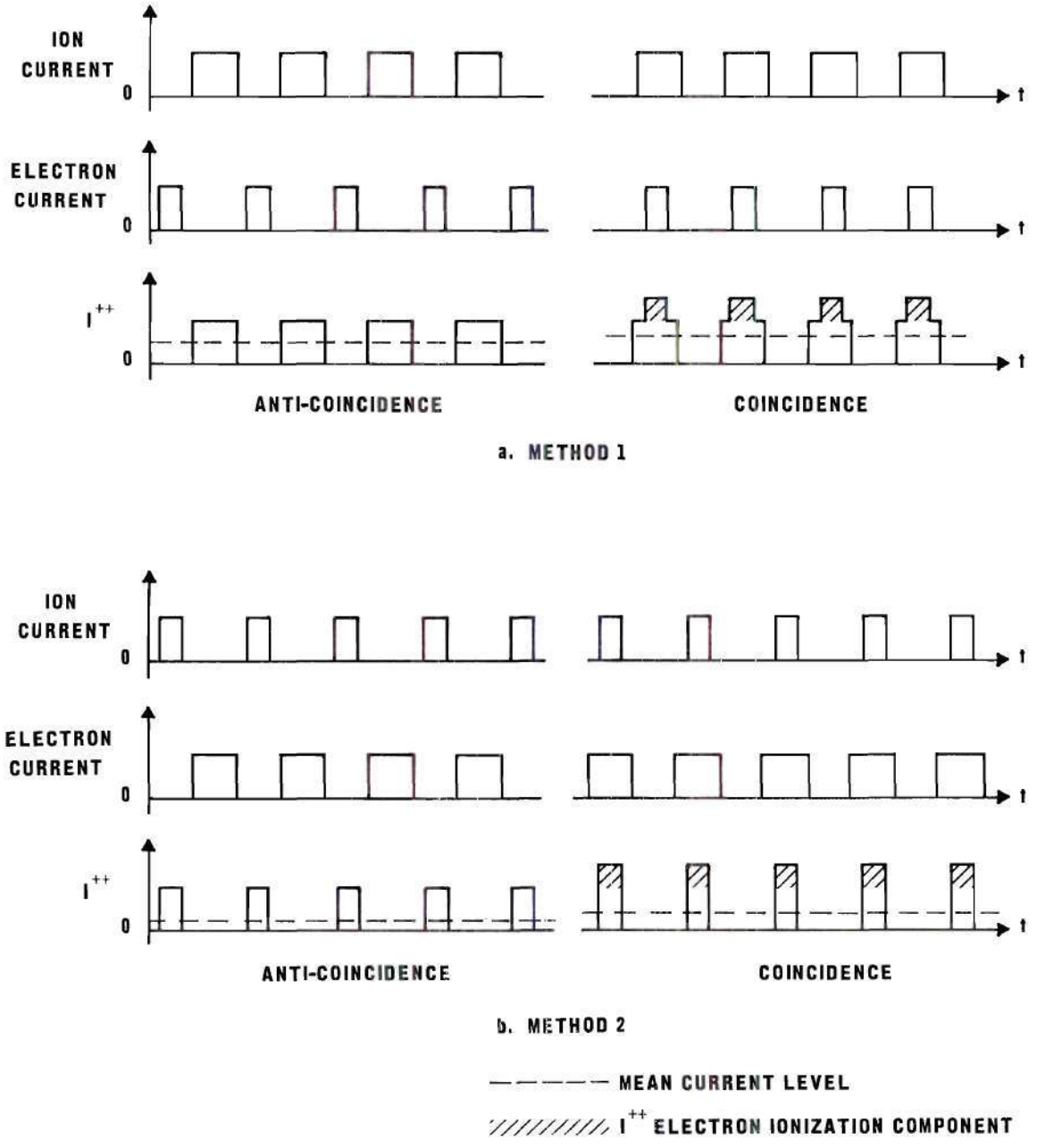

Figure 15. Current Waveforms Applicable when Both Ion and Electron Beams are Pulsed.

ion beam, thus giving rise to coincidence and anti-coincidence modes of operation. In the anti-coincidence mode, an ion current flows only when the electrons are cut off, and the I^{++} current consists only of the ion beam noise component. In the coincidence mode the electron beam crosses the interaction region only when ions are present, and the resulting I^{++} current contains both electron ionization and noise components. The difference in the mean current levels in these two modes is a measure of the electron impact ionization component; the fact that the desired signal information is contained in the mean current levels is the principal advantage of this pulsing scheme. Since only mean current levels are of importance, a sensitive instrument such as the vibrating capacitor electrometer may be employed for the measurements.

Using the parameters of our hypothetical experiment we evaluate the signal to noise ratio as follows.

$$SNR = \frac{I_c^{++} - I_{ac}^{++}}{I_{ac}^{++}} \tag{35}$$

$$= \frac{.625 \times 10^{-15} - .50 \times 10^{-15}}{.50 \times 10^{-15}}$$

$$= 0.25$$

where I_c^{++} and I_{ac}^{++} are the mean I^{++} currents in the coincidence and anti-coincidence modes respectively. This SNR is a factor of two worse than that obtained with continuous

beams under similar conditions; in addition the I^{++} currents which must be measured are a factor of two smaller in magnitude than in the continuous beam case.

A second coincidence — anti-coincidence measurement is possible if the duty cycles of the ion and electron beam are interchanged. The pulse shapes for this arrangement are shown in Figure 15b. The mode of operation is the same as before and the SNR is calculated to be

$$SNR = \frac{I_c^{++} - I_{ac}^{++}}{I_{ac}^{++}} \qquad (36)$$

$$= \frac{.375 \times 10^{-15} - .25 \times 10^{-15}}{.25 \times 10^{-15}}$$

$$= 0.5.$$

The SNR is seen to be equal to that obtained in the continuous beam measurements, but the current levels are lower by a factor of four. Dolder, Harrison and Thonemann did not appear to employ this latter pulsing scheme, but it would have improved their SNR by a factor of two.

In both of these pulsing schemes the converging effect of the electron beam is the same as it would be in the continuous beam case. The effect of electron beam space charge in any event must still be assessed. The fact that the I^{++} current levels in the pulsed beam measurements are lower than those in the continuous beam measurements is a direct

result of constraining the peak electron beam space charge product to be constant throughout the comparisons. This constraint is reasonable since the upper limit on useable electron beam intensities (and hence the upper limit for the SNR) is set by space charge.

Conclusions

The following principal conclusions can be drawn from this discussion.

(1) The continuous beam measurements are superior to any pulsed beam measurements, provided that pressure changes are not significant during the measurement process.

(2) The only advantage in pulsing beams lies in establishing a steady state pressure.

(3) Pulsing only the electron beam can provide useful measurements if a sufficiently sensitive phase-sensitive detector is available or if a multiplier is used in a pulse counting mode.

(4) The desired signal information cannot be obtained if only the ion beam is pulsed.

(5) Pulsing both ion and electron beams permits determination of the desired signal while requiring only measurement of mean current levels.

(6) Either the ion or the electron beam may have the smaller duty cycle in the double pulsing scheme. The ion beam duty cycle being the smaller gives a better SNR, but at the expense of reduced signal levels.

(7) The effect of electron beam space charge on the ion beam noise current is not assessed in any of these measurement schemes. This effect must still be considered before reliable measurements can be made.

APPENDIX V

SPACE CHARGE LIMITATIONS ON BEAM INTENSITIES

In order to determine the feasibility of a proposed crossed beam experiment, it is necessary to estimate the space charge limitation on maximum beam currents obtainable from a thermionic source. These maximum currents would then be used, together with the estimated magnitude of the cross section to be measured, to determine the expected level of the desired signal current. In the absence of a beam-confining magnetic field, the space charge limited current density in an infinite, parallel plane diode provides a useful estimate of the maximum attainable beam current in an experimental apparatus.

Consider such a diode with the cathode at ground potential, and the anode at potential V_0 volts. Further let us assume that the cathode can emit an unlimited quantity of particles, all possessing zero initial velocity. The emitted particles are assumed to have mass m kilograms and charge e coulombs. If the cathode-anode spacing is d meters, then the space charge limited current density, J_m, is given by the Child-Langmuir law[42].

$$J_m = \frac{4\varepsilon_o}{9}\sqrt{\frac{2e}{m}}\frac{V_o^{3/2}}{d^2} \quad \text{amperes/meter}^2, \tag{37}$$

where ε_o is the permittivity of free space in rationalized mks units.

As an example of the magnitude of the space charge limited current density, consider the case where the emitted particles are electrons, the applied voltage is 200 volts, and the cathode-anode spacing is 10^{-2} meters. In this case, Equation (37) predicts a space charge limited current density of approximately 6.6 ma/cm^2.

The Child-Langmuir law is frequently written in the form

$$J_m = K V^c \tag{38}$$

where K is a constant depending only on the m/e ratio of the emitted particles and the geometry of the device, and c is a constant which is approximately equal to 1.5. This form of the Child-Langmuir law is a convenient one to use, because this form has been found to be approximately valid for many space charge limited devices other than the simple one for which Equation (37) is valid. Equation (38) can be used to estimate the voltage-current characteristics of many space charge limited devices. In the present research, for example, if it is found that at electron energy E_1, the maximum useable electron current density is J_1, then at energy E_2 the maximum useable current density is given by

$$J_2 = \left[\frac{E_2}{E_1}\right]^{3/2} J_1 \ . \tag{39}$$

When restated in terms of the electron number densities corresponding to J_1 and J_2, Equation (2) reads

$$N_2 = \left[\frac{E_2}{E_1}\right] N_1 . \tag{40}$$

Therefore the electron number density at which source space charge limitations appear is directly proportional to the electron energy. These relationships, however, are only approximations intended to provide crude bounds on the maximum current densities attainable from thermionic electron or ion sources in a given situation. The effect of the space charge spreading of a beam after it has exited from its source must be determined empirically in a given piece of apparatus. Thus, for the crossed beam experiment reported herein, the final judgement as to the maximum useable electron beam intensity must rely upon a demonstration that the measured cross sections are independent of the electron beam intensity. For additional information on this subject, the reader is referred to the works of Pierce[43] and Klemperer[44,45], which will provide a guide to the extensive literature on electron optics.

BIBLIOGRAPHY*

1. H. Funk, Ann. Physik 4, 149 (1930).

2. R.L.F. Boyd and G. W. Green, Proc. Phys. Soc. (London) 71, 351 (1958).

3. W. L. Fite and R. T. Brackmann, Phys. Rev. 112, 1141 (1958).

4. K. T. Dolder, M. F. A. Harrison, and P. C. Thonemann, Proc. Roy. Soc. (London) A-264, 367 (1961).

5. K. T. Dolder, M. F. A. Harrison, and P. C. Thonemann, Proc. Roy. Soc. (London) A-274, 546 (1963).

6. K. T. Dolder, M. F. A. Harrison, and P. C. Thonemann, Proc. Phys. Soc. (London) 82, 368 (1963).

7. A. Burgess, Astrophys. J. 132, 503 (1960).

8. A. Burgess and M. R. H. Rudge, Proc. Roy. Soc. (London) A-273, 372 (1963).

9. E. W. Rothe, L. L. Marino, R. H. Neynaber, and S. M. Trujillo, Phys. Rev. 125, 582 (1962).

10. S. E. Kupriyanov and Z. Z. Latypov, Soviet Phys.-JETP 18, 558, (1964).

11. Z. Z. Latypov, S. E. Kupriyanov, and N. N. Tunitskiĭ, Soviet Phys.-JETP 19, 570 (1964).

12. W. A. Fowler, J. L. Greenstein, and F. Hoyle, Am. J. Phys. 29, 393 (1961).

13. W. A. Fowler, J. L. Greenstein, and F. Hoyle, Geophys. J. of the Royal Astronomical Society 6, 148 (1962).

14. H. Ishii and K. Nakayama, Transactions of the Eighth Vacuum Symposium, 1961 (Pergamon Press, Oxford, 1962), Vol. I, p. 519.

15. C. Meinke and G. Reich, Vacuum 13, 579 (1963).

---

*Abbreviations used herein conform to those found in the American Institute of Physics Style Manual (1963).

16. E. W. Rothe, J. Vac. Sci. and Tech. 1, 66 (1964).

17. Von W. Gaede, Ann. Physik 46, 357 (1915).

18. E. W. McDaniel, Collision Phenomena in Ionized Gases (John Wiley and Sons, Inc., New York, 1964), Chap. 13.

19. L. Holland, J. Sci. Instr. 38, 339 (1961).

20. J. Holden, L. Holland and L. Laurenson, J. Sci. Instr. 36, 281 (1959).

21. L. Elsworth, L. Holland and L. Laurenson, J. Sci. Instr. 37, 449 (1960).

22. W. Steckelmacher, Vacuum 12, 109 (1962).

23. O. W. Richardson, The Emission of Electricity from Hot Bodies, (Longmans Green and Co., London, 1916), second edition, 1921, Chap. VIII.

24. J. P. Blewett and E. J. Jones, Phys. Rev. 50, 464 (1936).

25. S. K. Allison and M. Kamegai, Rev. Sci. Instr. 32, 1090 (1961).

26. G. D. Yarnold and H. C. Bolton, J. Sci. Instr. 26, 38 (1949).

27. G. A. Harrower, Rev. Sci. Instr. 26, 850 (1955).

28. J. Van Eck, F. J. DeHeer and J. Kistemaker, Proceedings of the Fifth International Conference on Ionization Phenomena in Gases, Munich, 1961 (North-Holland, Amsterdam, 1962), Vol. I, p. 54.

29. K. Bethge, Z. Physik 162, 34 (1961).

30. C. Brunée, Z. Physik 147, 161 (1957).

31. J. J. Thomson, Phil. Mag. 23, 449 (1912).

32. G. Elwert, Z. Naturforsch. 7a, 432 (1952).

33. H. W. Drawin, Z. Physik 164, 513 (1961).

34. M. J. Seaton, Planet. Space Sci. 12, 55 (1964).

35. P. T. Smith, Phys. Rev. 36, 1293 (1930).

36. E. W. McDaniel, Collision Phenomena in Ionized Gases (John Wiley and Sons, Inc.,New York, 1964), Chap. 1.

37. W. H. Kohl, Materials and Techniques for Electron Tubes (Reinhold Publishing Corp., New York, 1960), pp. 556-7.

38. Tube Laboratory Manual (Research Laboratory of Electronics, Massachusetts Institute of Technology, Cambridge, Mass., 1956), 2nd ed., pp. 46-50.

39. G. A. Haas and J. T. Jensen, Jr., Rev. Sci. Instr. 28, 1007 (1957).

40. G. A. Haas and J. T. Jensen, Jr., Rev. Sci. Instr. 30, 562 (1959).

41. S. Dushman, Scientific Foundations of Vacuum Technique (John Wiley and Sons, Inc., New York, 1962), 2nd ed., p. 675.

42. R. L. Ramey, Physical Electronics (Wadsworth Publishing Co., Inc., Belmont, California, 1961), pp. 213-5.

43. J. R. Pierce, Theory and Design of Electron Beams (D. Van Nostrand Co., Inc., Princeton, New Jersey, 1954), second edition.

44. O. Klemperer, Electron Optics (Cambridge University Press, London, 1953), second edition.

45. O. Klemperer, Proc. Phys. Soc. (London) 59, 302 (1947).

VITA

William Carl Lineberger was born in Hamlet, North Carolina on December 5, 1939. He is the son of Mr. and Mrs. C. H. Lineberger. On August 19, 1961 he was married to Aileen Holden Jeffries, from Atlanta, Georgia.

Mr. Lineberger attended public schools in Charleston, South Carolina and Tampa, Florida; he was graduated from H. B. Plant High School in Tampa, Florida in 1957. He received the degrees of Bachelor of Electrical Engineering and Master of Science in Electrical Engineering in June, 1961 and June, 1963, both from the Georgia Institute of Technology.

Mr. Lineberger held a National Science Foundation Cooperative Graduate Fellowship from September, 1961 to September, 1962, and a National Aeronautics and Space Administration Traineeship from September, 1962 to April, 1965.

Mr. Lineberger is a member of the American Physical Society and of Sigma Xi.